
PEEKING INSIDE SPARSE NEURAL NETWORKS USING MULTI-PARTITE GRAPH REPRESENTATIONS

Elia Cunegatti

University of Trento, Italy
elia.cunegatti@unitn.it

Doina Bucur

University of Twente, The Netherlands
d.bucur@utwente.nl

Giovanni Iacca

University of Trento, Italy
giovanni.iacca@unitn.it

ABSTRACT

Modern Deep Neural Networks (DNNs) have achieved very high performance at the expense of computational resources. To decrease the computational burden, several techniques have proposed to extract, from a given DNN, efficient subnetworks which are able to preserve performance while reducing the number of network parameters. The literature provides a broad set of techniques to discover such subnetworks, but few works have studied the peculiar topologies of such pruned architectures. In this paper, we propose a novel *unrolled input-aware* bipartite Graph Encoding (GE) that is able to generate, for each layer in an either sparse or dense neural network, its corresponding graph representation based on its relation with the input data. We also extend it into a multipartite GE, to capture the relation between layers. Then, we leverage on topological properties to study the difference between the existing pruning algorithms and algorithm categories, as well as the relation between topologies and performance.

1 Introduction

Pruning Dense Neural Networks (DNNs) has recently become one of the most promising research areas in machine learning. Network pruning consists in removing a portion of network parameters (i.e., weights) aiming at reducing the computational resources and the inference time while avoiding performance degradation. Currently, one of the most important findings in network pruning [26] proved that, inside a randomly initialized DNN, there are subnetworks (the so-called “*winning tickets*”) that once trained in isolation can reach the performance of the overall dense network.

The algorithms proposed to find such subnetworks can be roughly split into four categories, which differ in *how* and *when* they uncover the sparse architecture. The earliest works focus on *Post-Training Pruning*, i.e., methods that, once the dense network has been fully trained, are able to uncover the sparse structures using simple heuristics to remove the lower-magnitude weights from the trained network [33, 50, 3, 19]. To decrease the computational cost of training the whole DNN, [54] and [46] propose a dense-to-sparse pruning technique employing Gradual Magnitude Pruning (GMP) to reduce the number of parameters during the training phase. The Lottery Ticket Hypothesis (LTH) [26] discovers the final sparse structure using an iterative process of training-pruning. A second group of algorithms focuses instead on *Pruning at Initialization (PaI)*, where the subnetwork is retrieved prior to training, based on a scoring criterion calculated on randomly initialized weights [35, 8, 37, 44, 1]. A third family of algorithms, called *Dynamic Sparse Training (DST)* techniques, aims at modifying the structure of the sparse network during the training process [18, 12, 34, 45, 14, 30]. The last category of pruning algorithms, based on the so-called *Strong Lottery Ticket Hypothesis (SLTH)*, differs from the previous categories since the weights are not trained at all [20, 49, 27].

Applying such pruning algorithms to a DNN $f(x, \theta)$ provides a binary mask $m \in \{0, 1\}^{|\theta|}$ that generates a Sparse Neural Network (SNN) $f(x, m \odot \theta)$ characterized by a certain topology. While many papers have investigated *how* to find sparse architectures, only a few looked at *why* (from a topological viewpoint) SNNs perform well, and *how* different pruning algorithms actually produce different SNN topologies. An SNN has indeed a unique topology, whose graph representation can be constructed and analyzed [31, 36]. The state-of-the-art in graph construction for SNNs with convolutional layers is based on *rolled* representations [17, 36, 13], where each node represents a layer parameter, i.e., either a filter/channel or a kernel value. However, such *rolled* representations do not capture the complete structure of the network. In fact, in these representations, the kernel parameters are used as static nodes. On the other hand,

convolutional operations use the kernel *dynamically* over the input data. The latter can be represented as nodes only in *unrolled* representations, see [4].

To overcome this limitation, we propose a novel *unrolled input-aware* Graph Encoding (GE) which fully represents the relation between the layer parameters and the layer input data. This encoding is radically different from all the *rolled* encodings previously proposed in the literature for the complete graph representation of convolutional layers. In particular, unlike the weighted *unrolled* GE proposed in [4], which is only designed to associate the weights of a DNN to graph edges, our proposed GE works with both dense and sparse architectures and focuses on the presence/absence of edges, rather than their weights. Furthermore, our GE generates one bipartite graph *for each layer*, rather than one bipartite graph *for each combination of input feature maps and filters*, as in [4]. Our GE works as follows: it takes as input a neural network (dense or sparse), and the input data size, and generates one bipartite graph for each layer. Nodes correspond to that layer’s inputs (e.g., in computer vision tasks, these are pixels in feature maps) while edges correspond to the masked/unmasked relation between those inputs and the output features, which in turn is based on the pruned layer parameters (in the case of SNNs; in the case of DNNs, all parameters are considered). We then extend this GE into a multipartite graph, to describe relations between layers.

Finally, we use the proposed GE to thoroughly study different categories of state-of-the-art unstructured pruning algorithms, to “peek inside” the SNNs they generate, and to understand how the *topological features* of those SNNs are related to their *performance drop* w.r.t. their corresponding DNNs, especially at extreme sparsity levels. We base our analysis on a large pool of SNNs obtained by combining eleven pruning algorithms, five sparsity ratios, three datasets, and four Convolutional Neural Networks (CNNs) benchmarked in the literature on SNNs, such as Conv-6 [26], as well as on state-of-the-art CNNs, such as ResNet [22], Wide-Resnet [53], and MobileNet [23, 38].

To summarize, the main contributions of this paper can be outlined as follows:

- (a) a novel *unrolled input-aware* GE which correctly reflects the convolutional operations, and links consecutive layers into a single multipartite graph representing the whole SNN;
- (b) an extensive study about how each pruning algorithm (and algorithm category) generates sparse topologies with similar patterns;
- (c) an analysis of which topological features can predict the performance drop of SNNs.

2 Related Work

We summarize the literature on pruning algorithms and graph representations of neural networks.

2.1 Pruning Algorithms

Pruning at Initialization. This set of algorithms aims at discovering the best subnetwork (prior to training) and selecting the weights based on some predefined criteria. The earliest approach of this kind is SNIP [35], which aims at selecting the weights based on their influence on the loss function. Moreover, an iterative version of SNIP is presented in [37]. GraSP [8] applies a gradient signal preservation mechanism based on Hessian-gradient product, while SynFlow [44] maximizes the synaptic strengths. More recently, ProsPR [1] has been devised in order to maximize the trainability throughout meta-gradients on the first steps of the optimization process. Lastly, NTK-SAP [51] uses neural tangent kernel theory to remove the less informative connections. These approaches are relatively cheap in terms of computational cost, since the mask is found before training. However, while increasing the sparsity ratios, the performances deteriorate faster than with other categories of pruning algorithms, due to the difficulty of training SNNs from scratch [16, 15] and to the fact that the architecture is statically determined and cannot change during the training phase.

Dynamic Sparse Training. This category of algorithms has been proposed to tackle the aforementioned limitations of PaI, thus allowing higher performance at the cost of a slight increase of the computational cost. Using gradient information retrieved during the training, sparse architectures can change their topology based on magnitude pruning followed by a pre-defined growth criteria e.g. based on random growth [12, 34], momentum [45], or absolute gradients [14]. To overcome the limitation of fixed layer-wise sparsity ratio, a few reparametrization techniques have been proposed [34, 45], in order to better allocate parameters over layers.

Sanity Checks. Recent works [43, 25] have questioned the ability of PaI algorithms to uncover the most effective architectures, stating that they rather focus on discovering the best *layer-wise sparsity ratios*. Their ability to improve performance over random pruning algorithms has been discussed in [39], which shows how even small perturbations of random pruning (Layer-wise Random Pruning such as ER [12] and ERK [14]) are able to outperform well-engineered PaI algorithms.

2.2 Graph Representation of Sparse and Dense Neural Networks

In order to gain insights from DNN topologies, several works have tried to devise weighted graph representations of the networks. Based on such representations, early-stopping criteria [4], customized initialization techniques [29], and performance predictors [47, 48] have been introduced.

What sets an SNN apart from a DNN is its unique topology, which can provide insight into its ability to solve a given task even when removing a portion of parameters. Grounded in graph theory, the random generation of small sparse structures for both Multi-Layer Perceptrons (MLPs) [6, 42] and CNNs [52] has been studied, showing that performance is associated with the *clustering coefficient* (which measures the capacity of nodes to cluster together) and the *average path length* of its graph representation (i.e., the average number of connections across all shortest paths).

To investigate the topological properties of SNNs, different metrics have been proposed. In [31], Graph-Edit-Distance has been used as a similarity measure, computed only on MLPs, to show how the graph topology evolves using a *Dynamic Sparse Training* algorithm such as SET [12]. By using Singular Vector Canonical Correlation Analysis, in [5, 2] it has been shown that different topologies are able to achieve similar performances. Clusterability has been taken into account in [17], showing that MLPs are more clusterable than CNNs. Finally, the performance of SNNs has been investigated via basic graph properties [41] and by means of Ramanujan graphs for PaI algorithms, indicating that performances are correlated to the graph connectivity [36] and can be predicted e.g. using the Iterative Mean Difference of Bound (IMDB) [13].

In all the works mentioned above, the graph representation of the convolutional layers is modelled either with a relational graph [52], or with a *rolled* encoding based only on the kernel parameters [36, 13], rather than on the relationship between the latter and the input data. To the best of our knowledge, so far only [4] proposed an *unrolled* GE but, besides the fact that it considers the network weights, this method generates several bipartite graphs for each convolutional layer, while our approach generates only one bipartite graph per layer. From a topological point of view, the approach from [4] has in fact two main limitations. Firstly, it does not make possible to directly calculate topological measures for any layer, since each graph contains only partial information about it. Secondly, since in the convolutional operations each j^{th} filter is convoluted with the a^{th} input feature map one by one, separating these operations does not allow computing the correct final contribution over the input data.

3 Methodology

In this section, we first introduce the novel *unrolled input-aware* graph encoding and its formulation in the *bipartite* version. We then extend it to the *multipartite* version, which links consecutive layers. Finally, we propose topological metrics that can be extracted from such GEs.

3.1 Bipartite Graph Encoding (BGE)

The proposed BGE encodes a neural network as a list of unweighted directed acyclic bipartite graphs $G = (G_1, \dots, G_N)$, with N the number of layers in the neural network. The individual graphs are not linked into a single graph. Our notation is summarized in Table 1.

Table 1: Notation used in the paper. We consider the case of vision tasks.

Symbol	Definition
$G = (L \cup R, E)$	bipartite graph with left node set L , right node set R (for a total of $ L + R $ nodes), and edge set E
N	number of layers
h, w	height and width of the input feature map
M	binary mask of pruned/unpruned weights
W	layer parameters
h_{ker}, w_{ker}	height and width of kernel
c_{in}, c_{out}	number of input and output channels
P, S	padding, stride

Due to its design, the bipartite graph construction differs for linear and convolutional layers. For linear layers, we use the encoding proposed in [4, 17, 47, 13]: denoting with L and R respectively the left and right layer of the i -th bipartite

graph, and given a binary mask $M_i \in \{0, 1\}^{|L_i| \times |R_i|}$, its corresponding GE is $G_i = (L_i \cup R_i, E_i)$, where E_i is the set of edges present in M_i , i.e., $(a, b) \in E_i \iff M_i^{a,b} \neq 0$.

For convolutional layers, our approach is substantially different from all the previous ones proposed in the literature. Specifically, we devise our encoding based on the *unrolled* input size: given as input, for each i -th layer, a set of feature maps $I_i \in \mathbb{R}^{h_i \times w_i \times c_{in}}$, we construct the corresponding bipartite graph as $G_i = (L_i \cup R_i, E_i)$, where again L_i and R_i are the two layers of the bipartite graph, and L_i corresponds to the flattened representation of the inputs. The size of the layer R_i , i.e., the output feature map, is calculated based on the input size I_i and the layer parameters $W_i \in \mathbb{R}^{c_{out} \times c_{in} \times h_{ker} \times w_{ker}}$:

$$|L_i| = h_i \times w_i \times c_{in} \quad |R_i| = \left(\frac{h_i - h_{ker}}{S} + 1 \right) \times \left(\frac{w_i - w_{ker}}{S} + 1 \right) \times c_{out}. \quad (1)$$

Differently from the linear layer case, the set of edges E cannot be directly computed from the convolutional mask $M_i \in \{0, 1\}^{c_{out} \times c_{in} \times h_{ker} \times w_{ker}}$ since the latter is dynamically computed over the input data:¹:

$$x_{i,j}^{out} = \sum_{in=0}^{c_{in}-1} \sum_{u=-h_{ker}}^{h_{ker}} \sum_{v=-w_{ker}}^{w_{ker}} I_{u,v}^{in} \times M_{i+u,j+v}^{out,in} \quad \forall out \in [0, c_{out}). \quad (2)$$

From Eq. (1), we know that $I_{u,v}^{in}$ and $x_{i,j}^{out}$ respectively correspond to a node $a_{(u+v) \times in} \in L_i$ and a node $b_{(i+j) \times out} \in R_i$, so in this case the edges of the bipartite graph are constructed during the convolutional operation such that:

$$E_i = \{(a_{(u+v) \times in}, b_{(i+j) \times out}) \mid M_{i+u,j+v}^{out,in} \neq 0 \quad \forall out, in, u, v\} \quad (3)$$

where the ranges of out, in, u, v are defined according to Eq. (1), and in and out are respectively the IDs of the input and the output channel taken into consideration for that convolutional step², and $i + u, j + v$ correspond to one kernel entry. Intuitively, given a layer l^i , each input element (e.g., in computer vision tasks, each pixel) represents a node in the graph, and the connection between an element of the input (denoted as a) and an element of the output feature map (denoted as b) is present if and only if during the convolutional operation, the contribution of a for generating b is not set to zero by the mask M_i in the kernel cell used to convolute the two pixels. An illustration of such encoding, which highlights the construction of the graph throughout the convolutional steps for both dense and sparse networks, is shown in Figure 1.

3.2 Multipartite Graph Encoding (MGE)

The bipartite GE described above has been devised to encode, independently, each single layer (either convolutional or linear) in a network. However, the limitation of this BGE lies in the lack of connections between consecutive (and, indirectly, non-consecutive) layers. As mentioned earlier, this limitation is however common to all the other GEs proposed in the literature [4, 47, 36, 13], that analyze the layers one by one, without connecting consecutive layers l_i and l_{i+1} . On the other hand, differently from the existing encodings, our bipartite GE can be straightforwardly extended into a multipartite GE, in order to encode the whole network as an *unweighted directed acyclic multipartite graph* $G = (G_1, \dots, G_N)$, where each pair of consecutive graphs G_i and G_{i+1} is linked such that $R_{G_i} = L_{G_{i+1}}$ ³. The set of edges for each partition G_i is computed as described in Section 3.1. However, an extension of the previous encoding is needed for connecting consecutive layers when a pooling operation is employed between them, as explained in Appendix C.

3.3 Topological Metrics

The unrolled GE proposed allows us to study the SNNs from a topological perspective, including a first theoretical analysis of the network connectivity between consecutive layers. We compute a number of *topological metrics* (in the following, referred to for brevity as *topometrics*) over SNN topologies. These topometrics can be broken down into three categories: two structural (that we call **local** and **regional** graph metrics), and one related to the **stability** of pruning.

¹The formula uses cross-correlation.

²In case of depth-wise separable convolution [23], the steps are only computed if $in = out$.

³The graph representation of residual connections is not taken into consideration since the number of parameters is much smaller compared to classical convolutional layers.

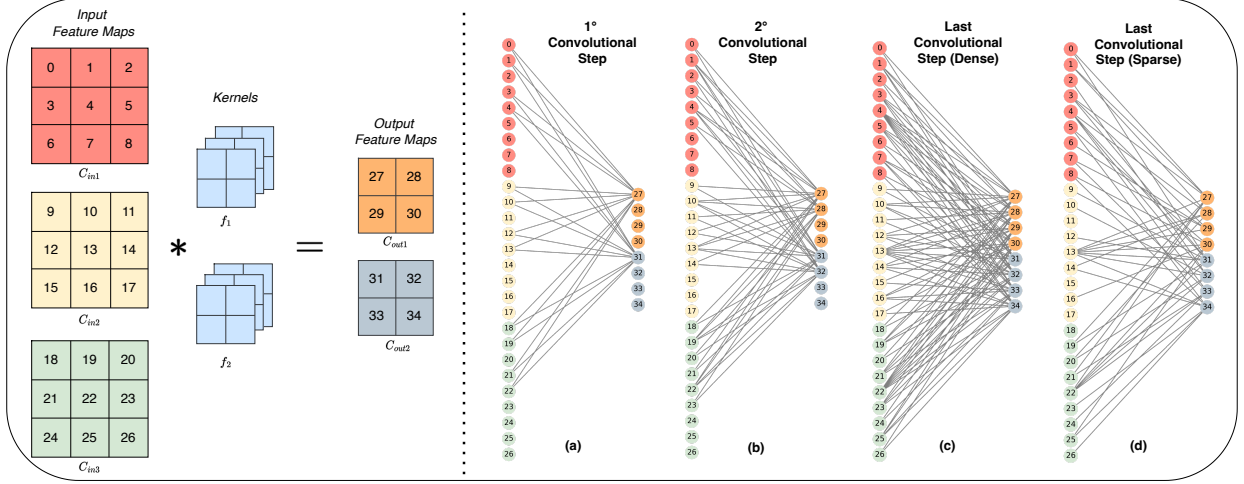


Figure 1: Illustration of the proposed unrolled input-aware BGE with $I = 3 \times 3 \times 3$ and convolutional parameters ($c_{out} = 2, c_{in} = 3, w_{ker} = 2, h_{ker} = 2, P = 0, S = 1$). (a) and (b) show, respectively, the first and second convolutional steps and how the graph edges are generated assuming that all the kernel parameters are unmasked. (c) shows the complete graph representation before pruning the kernel parameters. (d) shows the final graph representation after pruning the kernel parameters.

The **local** graph metrics are those computable over individual nodes or edges. These metrics (1) are computationally inexpensive, and (2) are able to capture some features of the graph connectivity between consecutive layers. Node-based topometrics include the fraction of *sink*, *source*, and *disconnected nodes* over the MGE. The sink and source⁴ nodes are, respectively, those with outdegree and indegree of zero. The disconnected nodes are those with neither incoming nor outgoing connections. Considering the sink and source nodes, it is possible to compute the fraction of *removable connections*, which are edge-based topometrics. The out-connections of the set of source nodes (denoted here α) are $r\text{-out} = \frac{1}{|E|} \cdot \sum_{n \in \alpha} \text{outdegree}(n)$. The in-connections of the set of sink nodes (denoted here β) are $r\text{-in} = \frac{1}{|E|} \cdot \sum_{n \in \beta} \text{indegree}(n)$. In fact, both these types of connections are useless for the final SNN performance, since they are ignored at inference.

The **regional** metrics are calculated over linked subgraphs in the MGE, such as $G = (G_i, G_{i+1})$ (hence any pair of consecutive BGEs, i.e., each tripartite slice). They (1) are more expensive computationally, but (2) can better analyze the connectivity of the networks. These topometrics are: the number of *motifs* (of size 3), the number of *connected components* (also known as clusters) and the *edge connectivity* (i.e., the number of “bridges” or edges to cut in order to disconnect the graph). Each topometric has been normalized based on the number of edges present in the graph representation—to prevent the graph size from being a confounding variable for the topological study conducted in Section 4.

The **stability** metrics are calculated in order to gain insights about how relevant (and stable) the graph edges are for a given task. These metrics, which we call *SJ* (Stability-Jaccard) and *SO* (Stability-Overlap), can be computed between any two graph representations of SNNs in two settings: 1) an *init* setting, where the pruning algorithm, sparsity ratio, and dataset are fixed, while the initialization seed is changed, and 2) a *data* setting, where the pruning algorithm, sparsity ratio, and initialization seed are fixed, while the input dataset is changed. These two metrics are computed over the graph edges respectively using the Jaccard distance (Intersection over Union) and the overlap coefficient (Szymkiewicz–Simpson):

$$SJ = \frac{\sum_{i=0}^N \frac{|E_i^1 \cap E_i^2|}{|E_i^1 \cup E_i^2|} \times e_i}{\sum_{i=0}^N e_i} \quad SO = \frac{\sum_{i=0}^N \frac{|E_i^1 \cap E_i^2|}{\min(|E_i^1|, |E_i^2|)} \times e_i}{\sum_{i=0}^N e_i} \quad (4)$$

where $e_i = \frac{|E_i^1| + |E_i^2|}{2}$. A value of either *SO* or *SJ* close to 1 has a different meaning per setting. In the *init* setting, it means that the pruning algorithm finds a topological structure which is not related to the values of the initialized weights. On the other hand, for the *data* setting a value close to 1 means that the algorithm finds the exact same topological structure independently from the input dataset.

⁴Padding nodes are already removed from the source set, since they have zero in-connections by design.

4 Experiments

In this section, we show how our proposed *input-aware unrolled GE* provides meaningful topometrics from graph representations of SNNs. We then use the topometrics for two purposes: 1) to classify both pruning algorithms and their categories, and 2) to develop a regression analysis to capture which topometrics can predict the accuracy drop of SNNs for different sparsity ratios. The first setting allows us to understand what makes SNNs produced by PaIs, DSTs and Layer-wise Random Pruning algorithms topologically different. The second setting allows us to understand how a certain sparse topology affects the architecture performance (from now on, we use “architecture” to refer to each CNN considered in our experimentation) and what may make some pruning algorithms perform better than others. It is worth mentioning that such analyses are based only on the unweighted graph representation of SNNs, hence do not take into consideration the weight values which could be highly dependent on the hyperparameters used in the training processes.

Experimental Setup. We generated a large pool of SNNs for our purposes. We use eleven different pruning algorithms: four Pruning at Initialization methods (Table 2), four Dynamic Sparse Training algorithms (Table 4), and three instances of Layer-wise Random Pruning (Table 3).

Table 2: Pruning at Initialization Algorithms.

Pruning Method	Drop	Sanity Check	Training Data	Iterative
SNIP [35]	$ \nabla_{\theta} L(\theta) $	\times	\checkmark	\times
GraSP[8]	$-H \nabla_{\theta} L(\theta)$	\times	\checkmark	\times
Synflow [44]	$\frac{\partial \mathcal{R}}{\partial \theta} \theta, \mathcal{R} = 1 \top (\prod_{l=1}^L \theta^l) 1$	\times	\times	\checkmark
ProsPr [1]	$ \nabla_{\theta_e} L(\theta_e) $	\times	\checkmark	\checkmark

Table 3: Random Pruning Algs.

Algorithm	Layer-wise Sparsity
Uniform [54]	$s^l \quad \forall l \in [0, N)$
ER [12]	$1 - \frac{n^{l-1} + n^l}{n^{l-1} \times n^l}$
ERK [14]	$1 - \frac{n^{l-1} + n^l + w^l + h^l}{n^{l-1} \times n^l \times w^l \times h^l}$

Table 4: Dynamic Sparse Training Pruning Algorithms.

Algorithm	Drop	Growth	Redistribution	Sparse Init.
DSR [34]	$ \theta $	random	random (zero layers)	Uniform
SNFS [45]	$ \theta $	momentum	momentum	Uniform
RigL [14]	$ \theta $	gradient	\times	ERK
SET-ITOP [32]	$ \theta $	random	\times	ERK

Since the graph size of the proposed GE is based on the size of the input data, we selected three datasets with the same data sizes, namely CIFAR-10, CIFAR-100 [28], and the downscaled Tiny-ImageNet (of size 32×32 pixels) [11]. We then used four different architectures designed for such input size, namely Conv-6 [26], Resnet-20 [22], Wide-Resnet-28-2 [53], and MobileNet-V2 [38]. We considered five sparsity values to cover a broad spectrum, namely $s \in [0.6, 0.8, 0.9, 0.95, 0.98]$ (as in [13]). We trained each combination of (pruning algorithm, dataset, architecture, sparsity) for 3 runs, obtaining a pool of 1,980 sparse architectures. More information on architectures, datasets, and hyperparameters is in Appendix A; the numerical results in terms of training accuracy (which correctly reproduce those reported in the literature) are in Appendix B.

The topometrics taken into consideration in the following experiments are the ones described in Section 3.3, namely: 1) *local* metrics, which consist of graph properties over nodes such as the fraction of source, sink, and disconnected nodes, plus metrics over edges, such as the fraction of removable connections (both in and out); 2) *regional* metrics, which consist of the number of motifs of size 3 over our directed acyclic multipartite graphs, the edge-connectivity (i.e., the percentage of bridge connections), and the number of clusters; 3) *stability* metrics, which are the *SJ* and *SO* metrics both for the *init* and the *data* settings; d) *combination*, which considers all these metrics together. For the classification and regression analysis, we use XGBoost [9].

4.1 Topological Classification

The first step in order to understand if different pruning algorithms provide either similar or diverse topologies is checking if the graph representation can be correctly classified based on its topological features. This analysis has been conducted for classifying both pruning algorithms and their categories (PaI, DST, Linear-wise Random Pruning). To do that, we average the topological properties of the SNNs obtained over different runs for the same combination (architecture, sparsity, dataset), in order to avoid overfitting, then we remove the duplicate entries. For each type of topometrics, we tested the classification accuracy over two different data subsets: 1) **Sparsity-wise**, i.e., we conduct the classification separately for each sparsity ratio, and 2) **Architecture-wise**, i.e., we conduct the classification separately

for each architecture. We also consider the case where all data are taken together (this case is referred to as “General”). We report the results in Table 5.

Table 5: Cross-validation balanced accuracy, using stratified k-fold with $k = 5$, for both pruning algorithm and algorithm category classification. The values have been averaged over 100 runs.

Classes	Topometrics	Accuracy (General)	Accuracy (Sparsity-wise)					Accuracy (Architecture-wise)			
			0.6	0.8	0.9	0.95	0.98	Conv-6	Resnet-20	Wide-Resnet-28-2	MobileNet-V2
Pruning category	Local	.75±.01	.66±.02	.71±.02	.73±.03	.81±.03	.85±.03	.76±.02	.67±.03	.79±.02	.93±.02
	Regional	.83±.02	.74±.03	.85±.03	.86±.03	.88±.03	.91±.02	.87±.02	.73±.03	.84±.03	.93±.02
	Stability	.76±.01	.79±.03	.83±.03	.76±.04	.80±.03	.79±.04	.76±.03	.74±.03	.72±.03	.77±.04
	Combination	.95±.01	.89±.03	.93±.03	.92±.03	.93±.02	.95±.02	.94±.02	.89±.02	.91±.03	.96±.02
Pruning algorithm	Local	.39±.01	.31±.02	.39±.02	.4±.03	.49±.03	.50±.04	.36±.03	.33±.03	.34±.03	.64±.03
	Regional	.49±.02	.57±.04	.57±.04	.53±.03	.55±.04	.58±.04	.60±.04	.44±.03	.52±.04	.60±.04
	Stability	.57±.02	.67±.03	.70±.03	.61±.04	.63±.03	.60±.04	.58±.03	.55±.03	.55±.03	.58±.03
	Combination	.72±.02	.74±.03	.80±.03	.73±.03	.72±.03	.70±.03	.73±.03	.65±.03	.66±.04	.71±.03

The results prove how different pruning algorithm categories generate SNNs with *different topological features*, which can be effectively classified with an average cross-validation balanced accuracy ~ 0.9 . It is also clear that the network topologies become more *separable* (i.e., the classification accuracy increases) with increasing sparsity ratio. For the classification of the pruning algorithms, the accuracy is computed over 11 classes, which means fewer samples per class available for training (compared to the classification by algorithm categories). However, on average, it is still possible to reach an accuracy ~ 0.7 . For both Sparsity-wise and Architecture-wise classification, the best results are achieved when all the topometrics are used all at once. In Appendix D, we report the feature importance scores for both the classification tasks in the “General” case.

4.2 Performance Prediction

The previous analysis showed that, from a classification perspective, different pruning algorithms (and categories thereof) generate network topologies with topological features. However, this analysis does not reveal how those features are associated with the **performance drop** of SNNs. It is already known that: 1) the performance drop is not always proportional to sparsity ratio, and 2) the performance of SNNs for some (sparsity, architecture, dataset) combinations could be even better than that of their dense counterparts [26, 25, 39]. Aiming at discovering associations between the topometrics and the performance drop, we conduct the following analysis. Starting from our pool of SNNs, we train a regression model and analyze its coefficient of determination R^2 (which is computed as $1 - \frac{\sum_i (y_i - \hat{y}_i)^2}{\sum_i (y_i - \bar{y})^2}$), which has been proved to be the most informative measure for discovering associations between input features and predicted variables [10]. For the regression, we use as inputs the same topometrics introduced before, and compute the performance drop as $1 - \frac{accuracy_s}{accuracy_d}$, where s and d respectively correspond to the sparse and deep version of any given architecture. We conduct this analysis separately for each dataset. This has been done due to the fact that the performance drop is highly related to the over-parametrization relation between the dataset and the architecture.

Then, for each dataset, we study the association between the topometrics and the performance drop for both the Sparsity-wise and Architecture-wise cases. These two analyses allow us to investigate from a topological perspective: 1) what makes certain SNNs, given the same fraction of parameters w.r.t. the dense version, perform better than others, and 2) what topological properties, for a given architecture, make its sparse version perform worse.

The R^2 coefficient values obtained using the *combination of all the proposed topometrics* are shown in Table 6. The results for each single category of topometrics (*local*, *regional* and *stability*) are available in Appendix D.2. Also for this study, the results reported are based on stratified cross-validation over 100 runs. To further assess the validity of our results, we also conducted an *ablation* study. For the Sparsity-wise case, we calculated the R^2 coefficient between architectures and corresponding performance drops separately for each value of sparsity ratio. For the Architecture-wise case, we calculated the R^2 coefficient between sparsity ratios and performance drops separately for each architecture. It can be clearly noticed that our topological approach reaches a R^2 coefficient much higher than that of the ablation studies, meaning that the proposed topometrics: 1) have a much higher predictive power than sparsity ratio and architecture alone, and 2) particularly for the Architecture-wise case, they add valuable information that is not captured when considering only the sparsity.

In addition, we analyzed the feature importance scores (using permutation importance) obtained during the regression analysis to find the most discriminative topometrics. Figure 2 (top-row) shows the feature importance for the Sparsity-wise case. The results have been averaged over 100 runs and then averaged over the three datasets (the results for each dataset are reported in Appendix D.2). For the Sparsity-wise case, the feature importance follows a clear pattern when increasing the sparsity ratio. Overall, the most discriminative feature turns out to be the number of motifs, i.e.,

Table 6: R^2 computed using stratified k-fold with $k = 5$ over 100 runs.

Dataset	Input features	R^2 (Sparsity-wise)					R^2 (Architecture-wise)			
		0.6	0.8	0.9	0.95	0.98	Conv-6	Resnet-20	Wide-Resnet-28-2	MobileNet-V2
CIFAR-10	Topometrics	.73±.04	.76±.07	.81±.05	.80±.09	.77±.07	.97±.01	.89±.03	.92±.02	.89±.05
	Architectures	.02±.02	.03±.02	.11±.06	.15±.07	.49±.07	-	-	-	-
	Sparsity ratios	-	-	-	-	-	.57±.06	.78±.02	.79±.03	.39±.08
CIFAR-100	Topometrics	.49±.07	.69±.07	.73±.05	.72±.08	.80±.05	.95±.02	.95±.01	.91±.02	.92±.04
	Architectures	.01±.01	.03±.02	.40±.06	.46±.07	.40±.06	-	-	-	-
	Sparsity ratios	-	-	-	-	-	.58±.03	.86±.01	.78±.03	.64±.05
Tiny-ImageNet	Topometrics	.74±.06	.88±.04	.86±.03	.85±.05	.81±.05	.93±.02	.91±.02	.92±.03	.89±.05
	Architectures	.23±.07	.51±.08	.51±.06	.57±.04	.55±.03	-	-	-	-
	Sparsity ratios	-	-	-	-	-	.52±.06	.78±.01	.63±.04	.69±.05

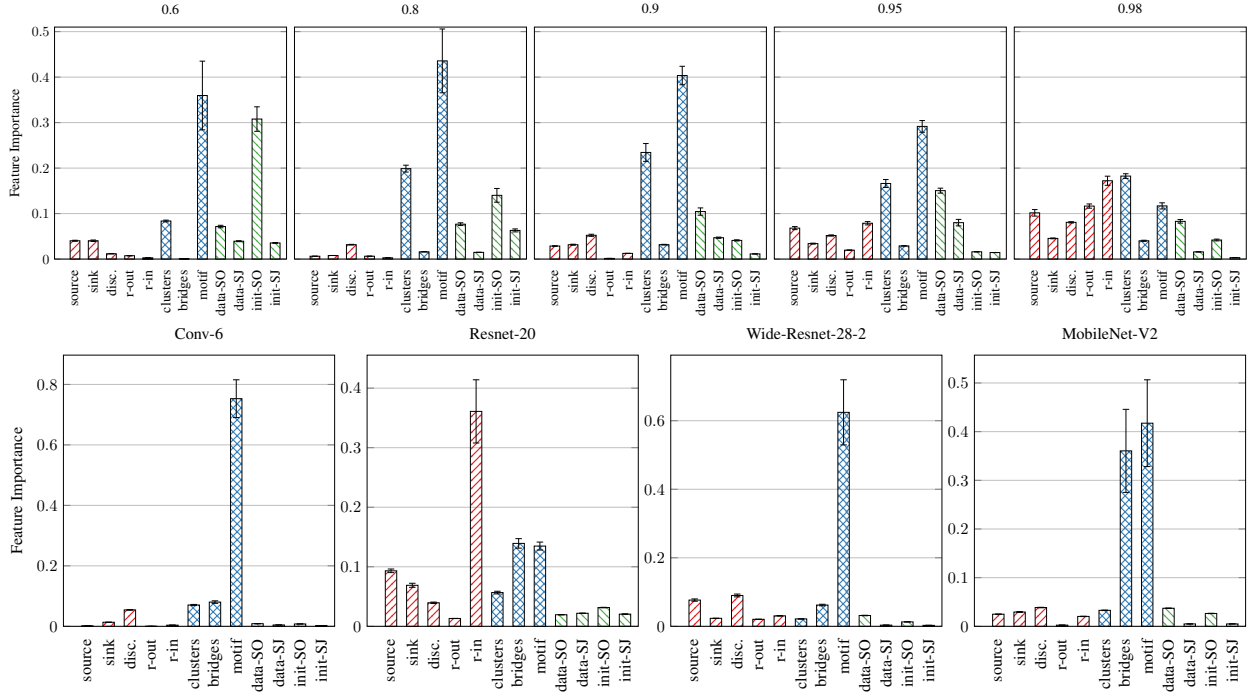


Figure 2: Feature importance scores for the regression analysis in the **Sparsity-wise (top row)** and **Architecture-wise (bottom row)** case. Colors highlight the contribution of different sets of metrics: *local* (red), *regional* (green), *stability* (blue).

the number of significant recurrent subgraphs of size 3 in the graph representation. Another clear trend regards the different categories of topometrics: as the sparsity ratio increases, the *local* metrics start to be more discriminative, while the *regional* and *stability* ones follow the inverse trend. Different sparsity ratios remove a different portion of parameters (and the corresponding edges in the graph representation) and disconnect the networks in different ways: for this reason, the feature importance scores “evolve” with the sparsity ratios. For instance, the importance of *clusters* and *removable connections* increases when the networks are sparser, therefore such metrics start to be effective in the regression analysis.

The same analysis was done over the Architecture-wise case, see Figure 2 (bottom-row), where the results previously discussed have been confirmed yet again. Also in this case, the number of motifs is the most discriminative feature, followed by edge connectivity (no. of bridges). It is also interesting to analyze how in a smaller network such as Resnet-20 (whose number of parameters is $\sim 0.1 - 0.2\%$ w.r.t. the other considered networks), the most discriminative feature turns out to be the number of removable connections. Overall, the metrics that are mostly associated with the performance drop are the ones related to network connectivity.

5 Conclusions

In this paper, we presented an in-depth analysis of the topologies of SNNs and their association with the performance drop. To do that, we studied the SNNs from a graph theory perspective, relying on a novel *unrolled input-aware* graph encoding which correctly reflects the convolutional steps and links across layers. The main limitation of our proposed GE is the time and space complexity for the encoding creation: for each layer of the MGE, i.e., for each BGE, the time complexity is $\mathcal{O}(c_{in} \times c_{out} \times step)$, while the space complexity is $\mathcal{O}(L + R + E)$, where $step = (\frac{L-d_{ker}}{S} + 1)^2$ and $|E| = c_{in} \times |W \setminus \{0\}| \times step$, assuming square feature maps and kernels.

On the other hand, we showed the practical applicability of our proposed GE through an analysis, both in terms of classification and prediction of the SNN performance based on topological metrics, of the most recent pruning algorithms from the literature.

Our findings are in line with the No-Free-Lunch-Theorem (NFLT) for pruning algorithms, i.e., “No single method is SOTA at initialization. Depending on the network, dataset, and sparsity, there is a setting where each early pruning method reaches the highest accuracy.” [25]. We in fact proved how, for the sake of accuracy prediction, the importance of most topometrics changes depending on the sparsity ratio and architecture. Even though association does not imply causation, our results suggest new hints to the NFLT, namely: 1) as we showed in our classification analysis, different pruning algorithms are designed differently, and, by construction, they generate SNNs with different topological features; 2) as shown in our performance prediction analysis, the topological features that are positively associated with the performance depend on the specific sparsity ratio and architecture, hence there is no guarantee that subnetworks found by any given pruning algorithm will perform well regardless of the sparsity ratio and architecture. Taken together, our analysis sheds therefore new light on the reason why the NFLT may hold true. However, while previous studies focused on the effects of the weights in SNNs, here we were able to investigate the properties and performance of the SNNs only looking at their topology, regardless of the weight values.

References

- [1] Alizadeh, Milad and Tailor, Shyam A. and Zintgraf, Luisa M and van Amersfoort, Joost and Farquhar, Sebastian and Lane, Nicholas Donald and Gal, Yarin. Prospect Pruning: Finding Trainable Weights at Initialization using Meta-Gradients. In *International Conference on Learning Representations*, 2022.
- [2] Ansuini, Alessio and Medvet, Eric and Pellegrino, Felice Andrea and Zullich, Marco. Investigating similarity metrics for convolutional neural networks in the case of unstructured pruning. In *International Conference on Pattern Recognition Applications and Methods*, pages 87–111. Springer, 2020.
- [3] Babak Hassibi and David G. Stork. Second Order Derivatives for Network Pruning: Optimal Brain Surgeon. In *Neural Information Processing Systems*, pages 164–171, 1992.
- [4] Bastian Rieck and Matteo Togninalli and Christian Bock and Michael Moor and Max Horn and Thomas Gumbsch and Karsten Borgwardt. Neural Persistence: A Complexity Measure for Deep Neural Networks Using Algebraic Topology. In *International Conference on Learning Representations*, 2019.
- [5] Blakeney, Cody and Yan, Yan and Zong, Ziliang. Is pruning compression?: Investigating pruning via network layer similarity. In *IEEE/CVF Winter Conference on Applications of Computer Vision*, pages 914–922, 2020.
- [6] Bourelly, Alfred and Boueri, John Patrick and Choromonski, Krzysztof. Sparse neural networks topologies, 2017. arXiv:1706.05683.
- [7] Cai, Yaohui and Hua, Weizhe and Chen, Hongzheng and Suh, G Edward and De Sa, Christopher and Zhang, Zhiru. Structured pruning is all you need for pruning CNNs at initialization, 2022. arXiv:2203.02549.
- [8] Chaoqi Wang and Guodong Zhang and Roger Grosse. Picking Winning Tickets Before Training by Preserving Gradient Flow. In *International Conference on Learning Representations*, 2020.
- [9] Chen, Tianqi and Guestrin, Carlos. XGBoost: A scalable tree boosting system. In *International Conference on Knowledge Discovery and Data Mining*, pages 785–794. ACM SIGKDD, 2016.
- [10] Davide Chicco, Matthijs J Warrens, and Giuseppe Jurman. The coefficient of determination R-squared is more informative than SMAPE, MAE, MAPE, MSE and RMSE in regression analysis evaluation. *PeerJ Computer Science*, 7:e623, 2021.
- [11] Chrabaszcz, Patryk and Loshchilov, Ilya and Hutter, Frank. A downsampled variant of ImageNet as an alternative to the CIFAR datasets, 2017. arXiv:1707.08819.

- [12] Decebal Constantin Mocanu and Elena Mocanu and Peter Stone and Phuong H. Nguyen and Madeleine Gibescu and Antonio Liotta. Scalable training of artificial neural networks with adaptive sparse connectivity inspired by network science. *Nature Communications*, 9, 2017.
- [13] Duc N.M Hoang and Shiwei Liu and Radu Marculescu and Zhangyang Wang. Revisiting Pruning At Initialization Through The Lens Of Ramanujan Graph. In *International Conference on Learning Representations*, 2023.
- [14] Evci, Utku and Gale, Trevor and Menick, Jacob and Castro, Pablo Samuel and Elsen, Erich. Rigging the lottery: Making all tickets winners. In *International Conference on Machine Learning*, pages 2943–2952. PMLR, 2020.
- [15] Evci, Utku and Ioannou, Yani and Keskin, Cem and Dauphin, Yann. Gradient flow in sparse neural networks and how lottery tickets win. In *AAAI Conference on Artificial Intelligence*, volume 36, pages 6577–6586, 2022.
- [16] Evci, Utku and Pedregosa, Fabian and Gomez, Aidan and Elsen, Erich. The Difficulty of Training Sparse Neural Networks. In *ICML Workshop on Identifying and Understanding Deep Learning Phenomena*, 2019.
- [17] Filan, Daniel and Casper, Stephen and Hod, Shlomi and Wild, Cody and Critch, Andrew and Russell, Stuart. Clusterability in neural networks, 2021. arXiv:2103.03386.
- [18] Guillaume Bellec and David Kappel and Wolfgang Maass and Robert A. Legenstein. Deep Rewiring: Training very sparse deep networks, 2017. arXiv:1711.05136.
- [19] Han, Song and Pool, Jeff and Tran, John and Dally, William. Learning both weights and connections for efficient neural network. In *Advances in Neural Information Processing Systems*, volume 28, pages 1135—1143, 2015.
- [20] Hattie Zhou and Janice Lan and Rosanne Liu and Jason Yosinski. Deconstructing Lottery Tickets: Zeros, Signs, and the Supermask. In *Neural Information Processing Systems*, 2019.
- [21] He, Kaiming and Zhang, Xiangyu and Ren, Shaoqing and Sun, Jian. Delving Deep into Rectifiers: Surpassing Human-Level Performance on ImageNet Classification. In *International Conference on Computer Vision*, pages 1026–1034, 2015.
- [22] He, Kaiming and Zhang, Xiangyu and Ren, Shaoqing and Sun, Jian. Deep residual learning for image recognition. In *IEEE/CVF Conference on Computer Vision and Pattern Recognition*, pages 770–778, 2016.
- [23] Howard, Andrew G and Zhu, Menglong and Chen, Bo and Kalenichenko, Dmitry and Wang, Weijun and Weyand, Tobias and Andreetto, Marco and Adam, Hartwig. MobileNets: Efficient convolutional neural networks for mobile vision applications, 2017. arXiv:1704.04861.
- [24] Ioffe, Sergey and Szegedy, Christian. Batch normalization: Accelerating deep network training by reducing internal covariate shift. In *International Conference on Machine Learning*, pages 448–456. PMLR, 2015.
- [25] Jonathan Frankle and Gintare Karolina Dziugaite and Daniel Roy and Michael Carbin. Pruning Neural Networks at Initialization: Why Are We Missing the Mark? In *International Conference on Learning Representations*, 2021.
- [26] Jonathan Frankle and Michael Carbin. The Lottery Ticket Hypothesis: Finding Sparse, Trainable Neural Networks. In *International Conference on Learning Representations*, 2019.
- [27] Kartik Sreenivasan and Jy-yong Sohn and Liu Yang and Matthew Grinde and Alliot Nagle and Hongyi Wang and Eric Xing and Kangwook Lee and Dimitris Papailiopoulos. Rare Gems: Finding Lottery Tickets at Initialization. In *Advances in Neural Information Processing Systems*, volume 35, pages 14529–14540, 2022.
- [28] Krizhevsky, Alex and Hinton, Geoffrey and others. Learning multiple layers of features from tiny images. Master’s thesis, University of Toronto, ON, Canada, 2009.
- [29] Limnios, Stratis and Dasoulas, George and Thilikos, Dimitrios M and Vazirgiannis, Michalis. Hcore-init: Neural network initialization based on graph degeneracy. In *International Conference on Pattern Recognition*, pages 5852–5858, 2021.
- [30] Liu, Shiwei and Chen, Tianlong and Chen, Xiaohan and Atashgahi, Zahra and Yin, Lu and Kou, Huanyu and Shen, Li and Pechenizkiy, Mykola and Wang, Zhangyang and Mocanu, Decebal Constantin. Sparse training via boosting pruning plasticity with neuroregeneration. In *Advances in Neural Information Processing Systems*, volume 34, pages 9908–9922, 2021.
- [31] Liu, Shiwei and Van der Lee, Tim and Yaman, Anil and Atashgahi, Zahra and Ferraro, Davide and Sokar, Ghada and Pechenizkiy, Mykola and Mocanu, Decebal Constantin. Topological insights into sparse neural networks. In *Joint European Conference on Machine Learning and Knowledge discovery in databases*, pages 279–294. Springer, 2021.
- [32] Liu, Shiwei and Yin, Lu and Mocanu, Decebal Constantin and Pechenizkiy, Mykola. Do we actually need dense over-parameterization? In-time over-parameterization in sparse training. In *International Conference on Machine Learning*, pages 6989–7000. PMLR, 2021.

- [33] Michael C. Mozer and Paul Smolensky. Skeletonization: A Technique for Trimming the Fat from a Network via Relevance Assessment. In *Neural Information Processing Systems*, pages 108–115, 1988.
- [34] Mostafa, Hesham and Wang, Xin. Parameter efficient training of deep convolutional neural networks by dynamic sparse reparameterization. In *International Conference on Machine Learning*, pages 4646–4655. PMLR, 2019.
- [35] Namhoon Lee and Thalaiyasingam Ajanthan and Philip Torr. SNIP: single-shot network pruning based on connection sensitivity. In *International Conference on Learning Representations*, 2019.
- [36] Pal, Bithika and Biswas, Arindam and Kolay, Sudeshna and Mitra, Pabitra and Basu, Biswajit. A Study on the Ramanujan Graph Property of Winning Lottery Tickets. In *International Conference on Machine Learning*, pages 17186–17201. PMLR, 2022.
- [37] Pau de Jorge and Amartya Sanyal and Harkirat Singh Behl and Philip H. S. Torr and Grégory Rogez and Puneet Kumar Dokania. Progressive Skeletonization: Trimming more fat from a network at initialization, 2020. arXiv:2006.09081.
- [38] Sandler, Mark and Howard, Andrew and Zhu, Menglong and Zhmoginov, Andrey and Chen, Liang-Chieh. Mobilenetv2: Inverted residuals and linear bottlenecks. In *IEEE/CVF Conference on Computer Vision and Pattern Recognition*, pages 4510–4520, 2018.
- [39] Shiwei Liu and Tianlong Chen and Xiaohan Chen and Li Shen and Decebal Constantin Mocanu and Zhangyang Wang and Mykola Pechenizkiy. The Unreasonable Effectiveness of Random Pruning: Return of the Most Naive Baseline for Sparse Training. In *International Conference on Learning Representations*, 2022.
- [40] Simonyan, Karen and Zisserman, Andrew. Very deep convolutional networks for large-scale image recognition, 2014. arXiv:1409.1556.
- [41] Stier, Julian and Darji, Harshil and Granitzer, Michael. Experiments on properties of hidden structures of sparse neural networks. In *International Conference on Machine Learning, Optimization, and Data Science*, pages 380–394. Springer, 2022.
- [42] Stier, Julian and Granitzer, Michael. Structural analysis of sparse neural networks. *Procedia Computer Science*, 159:107–116, 2019.
- [43] Su, Jingtong and Chen, Yihang and Cai, Tianle and Wu, Tianhao and Gao, Ruiqi and Wang, Liwei and Lee, Jason D. Sanity-checking pruning methods: Random tickets can win the jackpot. In *Advances in Neural Information Processing Systems*, volume 33, pages 20390–20401, 2020.
- [44] Tanaka, Hidenori and Kunin, Daniel and Yamins, Daniel L and Ganguli, Surya. Pruning neural networks without any data by iteratively conserving synaptic flow. In *Advances in Neural Information Processing Systems*, volume 33, pages 6377–6389, 2020.
- [45] Tim Dettmers and Luke Zettlemoyer. Sparse Networks from Scratch: Faster Training without Losing Performance, 2019. arXiv:1907.04840.
- [46] Trevor Gale and Erich Elsen and Sara Hooker. The State of Sparsity in Deep Neural Networks, 2019. arXiv:1902.09574.
- [47] Vahedian, Fatemeh and Li, Ruiyu and Trivedi, Puja and Jin, Di and Koutra, Danai. Convolutional Neural Network Dynamics: A Graph Perspective, 2021. arXiv:2111.05410.
- [48] Vahedian, Fatemeh and Li, Ruiyu and Trivedi, Puja and Jin, Di and Koutra, Danai. Leveraging the Graph Structure of Neural Network Training Dynamics. In *International Conference on Information & Knowledge Management*, pages 4545–4549. ACM, 2022.
- [49] Vivek Ramanujan and Mitchell Wortsman and Aniruddha Kembhavi and Ali Farhadi and Mohammad Rastegari. What’s Hidden in a Randomly Weighted Neural Network? In *IEEE/CVF Conference on Computer Vision and Pattern Recognition*, pages 11890–11899, 2019.
- [50] Yann LeCun and John S. Denker and Sara A. Solla. Optimal Brain Damage. In *Neural Information Processing Systems*, pages 598–605, 1989.
- [51] Yite Wang and Dawei Li and Ruoyu Sun. NTK-SAP: Improving neural network pruning by aligning training dynamics. In *International Conference on Learning Representations*, 2023.
- [52] You, Jiaxuan and Leskovec, Jure and He, Kaiming and Xie, Saining. Graph structure of neural networks. In *International Conference on Machine Learning*, pages 10881–10891. PMLR, 2020.
- [53] Zagoruyko, Sergey and Komodakis, Nikos. Wide residual networks, 2016. arXiv:1605.07146.
- [54] Zhu, Michael and Gupta, Suyog. To prune, or not to prune: exploring the efficacy of pruning for model compression, 2017. arXiv:1710.01878.

A Experimental Setup

A.1 Datasets

CIFAR-10/100 [28]. These two datasets are composed of 60,000 colour images each. These images are divided, respectively for the two datasets, into 10 and 100 classes. Each image has size of 32×32 pixels. On both datasets, 50,000 are used for training, while the remaining 10,000 are used for testing purposes.

Tiny-ImageNet [11]. The Tiny-ImageNet dataset consists of 100,000 colour images of size 64×64 pixels. These images are divided into 200 classes, with each class containing 500 images. The dataset is further split into three sets: a training set, a validation set, and a test set. Each class has 500 training images, 50 validation images, and 50 test images. In our experiments, we further downsample the images to 32×32 pixels in order to use the same architectures for all datasets. The downsampling has been devised using the Box algorithm⁵ with the same approach used in [11].

A.2 Architectures

Conv-6. This model is a scaled-down variant of VGG [40] with six convolutional and three linear layers. Max-Pooling operation is employed every two convolutional layers. Batch norm [24] is employed after every convolutional/linear layer. This model was devised for the first time in [26] and used as a benchmark in many recent studies on sparse models [20, 49, 36]. The total number of learnable weights in the model is $\sim 2.3\text{M}$.

Resnet-20. This model is a modification of the classical ResNet architecture. Originally proposed in [22], it has been designed to work with images of size 32×32 pixels. The implementation is based on a public codebase⁶. This model has been benchmarked in [25, 39, 1, 27]. The total number of learnable weights in the model is $\sim 270\text{K}$.

Wide-Resnet-28-2. This model is a modification of Wide-ResNet, and was originally proposed in [53]. The implementation is based on a public codebase⁷. This model has been benchmarked in [34, 45, 25, 27]. The total number of learnable weights in the model is $\sim 1.4\text{M}$.

MobileNet-V2. This model is a modification of MobileNet-V2 and has been developed for datasets with image size 32×32 . It has a stride set from 2 to 1, and a kernel size for the average pooling from 4 to 7. The implementation is based on a public codebase⁸. This model has been benchmarked in [14, 27, 7]. The total number of learnable weights in the model is $\sim 2.3\text{M}$.

Table 7: Architectures of the models used in our experiments.

Layer	Conv-6	Resnet-20	Wide-Resnet-28-2
Conv 1		$3 \times 3, 16$ Padding 1 Stride 1	$3 \times 3, 16$ Padding 1 Stride 1
Layer stack1	$\begin{bmatrix} 3 \times 3, 64 \\ 3 \times 3, 64 \end{bmatrix}$ Max-Pool	$\begin{bmatrix} 3 \times 3, 16 \\ 3 \times 3, 16 \end{bmatrix} \times 3$	$\begin{bmatrix} 3 \times 3, 32 \\ 3 \times 3, 32 \end{bmatrix} \times 4$
Layer stack2	$\begin{bmatrix} 3 \times 3, 128 \\ 3 \times 3, 128 \end{bmatrix}$ Max-Pool	$\begin{bmatrix} 3 \times 3, 32 \\ 3 \times 3, 32 \end{bmatrix} \times 3$	$\begin{bmatrix} 3 \times 3, 64 \\ 3 \times 3, 64 \end{bmatrix} \times 4$
Layer stack3	$\begin{bmatrix} 3 \times 3, 256 \\ 3 \times 3, 256 \end{bmatrix}$ Max-Pool	$\begin{bmatrix} 3 \times 3, 64 \\ 3 \times 3, 64 \end{bmatrix} \times 3$ Avg Pool kernel size 8	$\begin{bmatrix} 3 \times 3, 128 \\ 3 \times 3, 128 \end{bmatrix} \times 4$ Avg Pool kernel size 8
FC	256, 256, nclasses	64, nclasses	128, nclasses

⁵<https://patrykchrabaszcz.github.io/Imagenet32/>

⁶https://github.com/akamaster/pytorch_resnet_cifar10/blob/master/resnet.py

⁷<https://github.com/xternalz/WideResNet-pytorch/blob/master/wideresnet.py>

⁸<https://github.com/kuangliu/pytorch-cifar/blob/master/models/MobileNet-V2.py>

Table 8: Details of the MobileNet-V2 architecture.

Layer	MobileNet-V2
Conv1	3×3 , stride 1, padding 1
Conv2	$\begin{bmatrix} 1 \times 1, 32 \\ 3 \times 3, 32 \\ 1 \times 1, 16 \end{bmatrix} \times 1$
Conv3	$\begin{bmatrix} 1 \times 1, 96 \\ 3 \times 3, 96 \\ 1 \times 1, 24 \end{bmatrix} \times 1$
Conv4	$\begin{bmatrix} 1 \times 1, 144 \\ 3 \times 3, 144 \\ 1 \times 1, 24 \end{bmatrix} \times 1$
Conv5	$\begin{bmatrix} 1 \times 1, 144 \\ 3 \times 3, 144 \\ 1 \times 1, 32 \end{bmatrix} \times 1$
Conv6	$\begin{bmatrix} 1 \times 1, 192 \\ 3 \times 3, 192 \\ 1 \times 1, 32 \end{bmatrix} \times 2$
Conv7	$\begin{bmatrix} 1 \times 1, 192 \\ 3 \times 3, 192 \\ 1 \times 1, 64 \end{bmatrix} \times 1$
Conv8	$\begin{bmatrix} 1 \times 1, 384 \\ 3 \times 3, 384 \\ 1 \times 1, 64 \end{bmatrix} \times 3$
Conv9	$\begin{bmatrix} 1 \times 1, 384 \\ 3 \times 3, 384 \\ 1 \times 1, 96 \end{bmatrix} \times 1$
Conv10	$\begin{bmatrix} 1 \times 1, 576 \\ 3 \times 3, 576 \\ 1 \times 1, 96 \end{bmatrix} \times 2$
Conv11	$\begin{bmatrix} 1 \times 1, 576 \\ 3 \times 3, 576 \\ 1 \times 1, 160 \end{bmatrix} \times 1$
Conv12	$\begin{bmatrix} 1 \times 1, 960 \\ 3 \times 3, 960 \\ 1 \times 1, 160 \end{bmatrix} \times 2$
Conv13	$\begin{bmatrix} 1 \times 1, 960 \\ 3 \times 3, 960 \\ 1 \times 1, 320 \end{bmatrix} \times 1$
	Avg Pool, kernel size 4
FC	1028, n_{classes}

A.3 Hyperparameters

We use a different hyperparameter setting for each category of pruning algorithms, following the suggested settings in the related literature (see below for details). The only hyperparameter that is in common for all the algorithms and datasets is the batch size, fixed to 128. Furthermore, random cropping (32×32 , padding 4) and horizontal flipping, has been used for data augmentation in all the experiments. In all cases, the weights have been initialized using the standard Kaiming Normal [21]. In the following, we detail the hyperparameters used for all the tested datasets and sparsity values.

A.3.1 Pruning at Initialization and Layer-wise Random Pruning

For the experiments with PaI and Layer-wise Random Pruning algorithms, as well as for the dense baselines, for CIFAR-10 and CIFAR-100 we train the models for 160 epochs with SGD with momentum 0.9. The initial learning rate is set to 0.1 and decreased by 10 at epochs 80 and 120. Weight decay is set to 1×10^{-4} for all models but Wide-Resnet-28-2, where it is set to 1×10^{-5} . For Tiny-ImageNet, we train the model for 100 epochs. The initial learning rate is set to 0.1 and decreased by 10 at epochs 30, 60, and 80. Momentum and weight decay hyperparameters are set as for CIFAR-10/100. This experimental setup is based on the ones used in [8, 44, 39].

A.3.2 Dynamic Sparse Training

In all the experiments with DST, we use the same hyperparameter settings regardless of the models and datasets. We train the models for 200 epochs, starting with a learning rate of 0.1 and decreasing it by 10 every 50 epochs. We use SGD with momentum set at 0.9 and weight decay at 1×10^{-5} . We start the training with a pruning rate of 0.3 which then decays by a cosine schedule until the last epoch. The update interval (ΔT) is set to 100 iterations for all the algorithms but SET-ITOP, where it is set to 1500 as proposed in the original paper [32]. The experimental setup is based on the ones used in [45, 14, 32].

A.4 Implementation

In order to replicate the results of all the pruning algorithms used in this paper, we based our code on the original PyTorch algorithm implementation whenever possible. Sources are the following:

- SNIP <https://github.com/mil-ad/snip>
- GraSP <https://github.com/alecwangcq/GraSP>
- SynFlow <https://github.com/ganguli-lab/Synaptic-Flow>
- ProsPR <https://github.com/mil-ad/prospr>
- DSR and SNFS https://github.com/TimDettmers/sparse_learning
- ITOP <https://github.com/Shiweiliuuiiiiiii/In-Time-Over-Parameterization>
- RigL <https://github.com/nollied/rigl-torch>⁹
- Uniform, ER and ERK <https://github.com/VITA-Group/Random-Pruning>

B Results

In this section, the results of the experiments explained in Appendix A are shown separately for each dataset, see Tables 9-11. Each combination ⟨dataset, architecture, sparsity, pruning algorithm⟩ has been evaluated over 3 runs. We trained the models on a cluster with 8 NVIDIA A100 GPUs. The approximate runtime for the overall experimentation was around 25 days. In the tables, the symbol “*” indicates that the sparse network is not able to outperform the random dense baseline (i.e., if the probability of correctly guessing a sample class is $\frac{1}{C}$, the network after pruning has an average accuracy $\leq \frac{1}{C}$). This happens either for layer collapse, as in SNIP [35], ProsPR [1], and SynFlow [44], or due to the inability of layer reparametrization, as in DSR [34] and SNFS [45]. These phenomena appear only for $s = 0.98$ on MobileNet-V2, that is known to be difficult to prune due to its separable convolutions layers [54, 14]. In each table, for any combination ⟨architecture, sparsity, pruning category⟩, the best-performing algorithm is highlighted in boldface.

⁹Original Codebase in TensorFlow here <https://github.com/google-research/rigl>

Table 9: Accuracy results on CIFAR-10.

Sparsity Ratio	Conv-6						Resnet-20						Wide-Resnet-28-2						MobileNet-V2					
	0.6	0.8	0.9	0.95	0.98		0.6	0.8	0.9	0.95	0.98		0.6	0.8	0.9	0.95	0.98		0.6	0.8	0.9	0.95	0.98	
SNIP [35]	92.7±0.3	92.0±0.1	91.1±0.1	89.6±0.2	83.8±0.3	90.5±0.4	89.0±0.3	87.0±0.3	87.0±0.0	83.2±0.4	75.9±0.4	94.1±0.2	93.2±0.2	92.2±0.2	90.6±0.2	87.2±0.2	93.3±0.1	92.5±0.2	93.7±0.2	93.3±0.1	92.5±0.1	91.6±0.1	90.4±0.9	*
GradSP [8]	92.5±0.1	91.6±0.1	90.7±0.1	89.5±0.1	86.0±0.3	90.2±0.1	89.1±0.3	87.1±0.3	87.1±0.2	84.4±0.0	77.1±0.2	94.0±0.2	94.0±0.1	91.9±0.1	91.9±0.1	87.7±0.3	92.7±0.1	92.3±0.2	92.7±0.1	92.3±0.2	91.6±0.1	90.4±0.9	88.3±0.3	
SynFlow [44]	92.7±0.3	91.7±0.3	91.3±0.3	89.8±0.2	86.8±0.2	90.5±0.2	89.4±0.1	86.4±0.3	81.8±0.2	76.2±0.3	93.3±0.3	94.0±0.1	92.6±0.2	90.4±0.2	86.4±0.2	91.9±0.1	90.8±0.5	90.4±0.2	91.9±0.1	90.8±0.5	89.4±0.6	85.7±1.7	78.2±3.3	
ProSPR [1]	92.5±0.3	91.7±0.3	91.3±0.3	89.2±0.3	85.3±0.5	90.6±0.2	89.4±0.1	86.4±0.3	81.8±0.2	76.2±0.3	93.3±0.3	94.0±0.1	92.6±0.2	90.4±0.2	86.4±0.2	91.9±0.1	90.8±0.5	90.4±0.2	91.9±0.1	90.8±0.5	89.4±0.6	85.7±1.7	78.2±3.3	*
Uniform [54]	92.3±0.2	91.1±0.1	89.2±0.1	86.4±0.4	79.7±0.1	90.1±0.1	88.2±0.4	85.5±0.3	77.7±0.2	54.7±6.9	93.5±0.1	93.8±0.1	92.5±0.0	90.9±0.0	89.0±0.1	84.3±0.6	92.4±0.1	90.2±0.2	92.4±0.1	90.2±0.2	86.6±0.2	76.5±0.6	48.7±0.1	
ER [12]	91.3±0.1	90.2±0.1	88.6±0.2	86.5±0.1	82.7±0.2	90.5±0.2	89.1±0.1	86.9±0.3	83.8±0.2	77.0±0.3	93.8±0.1	93.2±0.2	92.1±0.1	90.4±0.2	87.0±0.0	93.5±0.2	93.0±0.1	92.0±0.3	93.5±0.2	93.0±0.1	92.0±0.3	89.8±0.3	82.8±0.2	
ERK [14]	91.3±0.1	90.2±0.2	88.8±0.3	86.7±0.1	82.5±0.1	90.8±0.3	89.4±0.3	87.1±0.1	83.8±0.2	77.4±0.2	94.1±0.1	93.4±0.1	92.2±0.3	90.4±0.2	86.9±0.2	93.6±0.0	93.2±0.1	92.2±0.0	93.6±0.0	93.2±0.1	92.2±0.0	90.0±0.2	83.0±0.3	
DSR [34]	93.3±0.3	93.0±0.1	92.4±0.3	91.4±0.3	89.3±0.1	91.3±0.1	90.7±0.2	89.3±0.2	86.8±0.7	80.4±1.0	93.7±0.1	93.3±0.1	92.7±0.2	91.7±0.1	89.7±0.2	92.5±0.1	92.0±0.1	92.0±0.1	92.5±0.1	92.4±0.2	91.4±0.2	90.1±0.5	*	
SNFS [45]	93.7±0.1	93.1±0.2	92.4±0.1	91.6±0.1	89.4±0.3	91.5±0.2	90.4±0.1	89.0±0.1	85.2±0.4	72.7±0.8	94.2±0.1	93.6±0.2	92.9±0.1	91.8±0.1	89.8±0.1	92.6±0.1	92.4±0.2	91.6±0.2	92.6±0.1	92.4±0.2	91.6±0.2	90.5±0.1	*	
RigL [4]	92.9±0.2	92.2±0.3	91.1±0.1	89.7±0.1	87.5±0.3	91.6±0.2	90.6±0.3	88.9±0.2	86.5±0.1	81.9±0.5	94.3±0.1	93.6±0.1	92.9±0.1	91.6±0.2	89.7±0.3	92.5±0.1	92.3±0.4	91.8±0.1	92.3±0.4	91.8±0.1	91.8±0.1	91.1±0.3	86.5±0.5	
SET-ITOP [32]	92.7±0.1	91.8±0.1	90.5±0.4	88.6±0.3	85.8±0.1	91.6±0.0	90.7±0.2	89.1±0.0	86.3±0.1	81.3±0.7	94.3±0.0	93.5±0.2	92.9±0.1	91.6±0.2	89.5±0.2	92.5±0.1	92.6±0.0	91.8±0.2	92.5±0.1	92.6±0.0	91.8±0.2	91.0±0.4	87.3±0.4	
Dense (Baseline)			93.2±0.0						91.7±0.1				94.4±0.1									93.8±0.2		

Table 10: Accuracy results on CIFAR-100.

Sparsity Ratio	Conv-6						Resnet-20						Wide-Resnet-28-2						MobileNet-V2					
	0.6	0.8	0.9	0.95	0.98		0.6	0.8	0.9	0.95	0.98		0.6	0.8	0.9	0.95	0.98		0.6	0.8	0.9	0.95	0.98	
SNIP [35]	66.9±0.5	65.2±0.4	62.8±0.7	56.7±1.4	38.2±1.8	64.3±0.2	60.6±1.1	52.5±1.5	41.9±0.9	24.4±0.5	72.4±0.2	70.4±0.2	67.8±0.2	63.2±0.3	64.2±0.6	55.1±1.1	73.4±0.4	72.2±0.3	73.4±0.4	72.2±0.3	68.1±0.4	*	66.0±0.4	54.4±1.7
GradSP [8]	66.5±0.3	64.5±0.4	62.6±0.2	59.6±0.1	52.2±0.5	63.7±0.3	60.4±0.3	54.2±0.3	45.9±0.1	31.2±1.3	71.9±0.3	69.9±0.5	67.7±0.3	62.6±0.6	63.2±0.6	55.1±1.1	71.9±0.2	70.6±0.1	71.9±0.2	70.6±0.1	68.8±0.5	66.0±0.4	54.4±1.7	
SynFlow [44]	67.4±0.3	65.1±0.0	63.2±0.3	60.8±0.2	54.7±0.1	63.9±0.1	58.9±0.4	50.1±0.1	38.2±0.6	19.2±2.5	71.8±0.2	69.3±0.5	66.1±0.4	60.5±0.0	60.5±0.0	48.7±0.3	70.9±0.4	66.8±0.5	70.9±0.4	66.8±0.5	60.2±2.3	44.9±0.0	*	
ProSPR [1]	67.3±0.3	64.8±0.6	62.9±0.2	59.6±0.1	52.2±0.4	64.1±0.1	60.0±0.7	49.4±2.9	26.8±5.3	26.5±1.1	72.4±0.5	70.5±0.3	67.9±0.3	61.5±0.4	61.5±0.4	45.1±3.2	73.0±0.1	71.7±0.0	73.0±0.1	71.7±0.0	69.7±0.7	66.0±1.0	*	
Uniform [54]	66.4±0.2	63.6±0.4	59.9±0.1	54.8±0.6	43.6±1.2	63.1±0.3	59.5±0.4	52.2±0.8	39.1±3.0	18.2±0.9	72.0±0.2	69.7±0.5	67.2±0.1	62.7±0.5	62.7±0.5	45.6±2.0	71.3±0.5	67.5±0.5	71.3±0.5	67.5±0.5	60.7±1.3	45.7±0.5	*	
ER [12]	64.8±0.3	62.3±0.1	59.9±0.4	55.6±0.1	47.5±0.8	64.6±0.5	61.4±0.2	55.8±0.2	47.2±0.5	33.7±0.5	72.2±0.4	68.0±0.6	64.1±0.4	61.1±0.4	61.1±0.4	56.1±0.4	73.1±0.5	71.1±0.3	73.1±0.5	71.1±0.3	69.3±0.3	64.9±0.2	50.1±0.3	
ERK [14]	65.1±0.5	62.0±0.1	59.0±0.4	56.0±0.2	47.3±0.1	65.4±0.5	61.8±0.2	55.8±1.2	47.3±0.1	33.6±0.6	70.7±0.1	68.1±0.1	64.7±0.6	60.3±0.1	60.3±0.1	56.3±0.1	73.9±0.4	71.6±0.1	73.9±0.4	71.6±0.1	69.3±0.2	65.2±0.2	50.4±0.8	
DSR [34]	69.6±0.6	68.6±0.3	65.4±0.2	65.7±0.2	59.7±0.2	65.4±0.4	61.2±0.1	57.7±0.2	52.4±2.3	39.2±1.6	72.3±0.3	69.6±0.2	67.8±0.2	67.6±0.6	67.6±0.6	61.8±0.4	71.1±0.6	70.9±0.3	71.1±0.6	70.9±0.3	69.9±0.2	64.9±0.8	*	
SNFS [45]	70.0±0.3	68.7±0.2	67.8±0.2	65.6±0.2	61.4±0.2	66.2±0.1	63.5±0.3	58.8±0.2	40.8±1.1	25.1±1.5	72.4±0.2	71.1±0.3	69.1±0.1	66.7±0.5	66.7±0.5	58.7±1.1	71.3±0.2	70.6±0.1	71.3±0.2	70.6±0.1	70.1±0.4	66.0±0.3	*	
RigL [4]	69.0±0.3	67.4±0.2	65.5±0.7	63.0±0.4	58.0±0.3	66.2±0.2	63.8±0.5	60.0±0.5	52.2±0.2	36.1±1.4	72.6±0.3	71.1±0.3	69.4±0.4	67.6±0.3	67.6±0.3	62.0±0.5	71.1±0.2	70.9±0.2	71.1±0.2	70.9±0.2	70.1±0.2	67.9±0.7	55.3±0.3	
SET-ITOP [32]	68.7±0.1	66.7±0.2	64.5±0.3	61.0±0.4	54.5±0.1	66.1±0.6	64.5±0.3	59.7±0.6	52.2±0.1	40.3±0.1	72.8±0.3	71.3±0.3	70.0±0.6	67.5±0.1	61.3±0.6	71.5±0.2	71.2±0.3	71.2±0.3	71.5±0.2	71.2±0.3	70.2±0.2	68.0±0.2	58.2±0.9	
Dense (Baseline)			68.5±0.2					66.4±0.3				74.2±0.2									74.3±0.4			

Table 11: Accuracy results on Tiny-ImageNet.

Sparsity Ratio	Conv-6					Resnet-20					Wide-Resnet-28-2					MobileNet-V2				
	0.6	0.8	0.9	0.95	0.98	0.6	0.8	0.9	0.95	0.98	0.6	0.8	0.9	0.95	0.98	0.6	0.8	0.9	0.95	0.98
SNIP [35]	45.9±0.2	43.7±0.6	37.3±0.2	29.2±1.0	16.6±1.5	41.5±0.3	34.2±1.5	27.2±0.5	19.8±0.3	10.8±0.6	48.7±0.3	47.8±0.3	44.5±0.9	38.3±0.8	27.8±0.6	53.7±0.5	50.5±0.1	36.3±1.5	*	0.98
GnsSP [8]	45.2±0.5	44.5±0.4	42.6±0.5	39.0±0.3	31.6±0.4	41.1±0.4	36.4±0.6	30.5±0.2	23.2±1.2	13.0±0.4	47.8±0.8	46.9±0.7	44.0±0.3	39.3±0.4	20.8±0.7	52.0±0.5	51.0±0.2	48.8±0.3	43.6±0.3	27.3±2.5
SynFlow [44]	46.2±0.2	45.0±0.3	43.2±0.4	40.0±0.3	32.6±0.7	41.4±0.1	33.7±0.4	24.4±0.3	13.9±0.4	6.1±0.8	48.5±0.5	46.0±0.1	41.2±0.4	33.6±0.5	21.2±0.9	52.0±0.5	51.0±0.2	47.5±1.1	24.7±2.3	*
ProSPR [1]	46.3±0.4	45.7±0.9	43.1±0.4	39.3±0.3	31.8±0.8	40.4±1.1	34.6±0.1	22.0±1.0	9.2±2.5	7.1±5.2	49.3±0.3	47.1±0.4	43.8±0.3	34.9±0.9	27.5±0.1	48.7±0.1	48.5±0.4	46.3±0.6	40.4±0.1	*
Uniform [54]	45.6±0.5	43.8±0.3	40.3±0.3	34.9±0.4	25.7±0.2	40.4±0.1	35.3±0.3	28.5±0.3	20.5±0.4	9.3±1.4	47.7±0.9	46.1±0.4	41.7±0.8	36.0±0.4	25.3±0.9	51.9±0.4	48.5±0.5	40.8±0.2	28.7±0.7	*
ER [12]	44.4±0.4	43.7±0.2	40.3±0.4	36.3±0.5	28.5±0.4	43.1±0.7	37.8±0.3	32.2±0.4	25.6±0.2	15.1±0.4	49.3±0.4	48.0±0.2	44.6±0.3	39.9±0.4	31.5±0.3	53.6±0.5	52.2±0.1	50.4±0.4	44.2±0.4	31.1±0.4
ERK [14]	44.1±0.3	43.0±0.4	40.9±0.1	35.8±0.2	28.6±0.3	43.8±0.5	38.6±0.4	32.1±0.0	25.4±0.2	15.6±0.2	48.9±0.2	48.1±0.2	44.4±0.4	39.6±0.5	31.6±0.5	53.4±0.5	52.5±0.3	49.7±0.2	44.1±0.5	30.9±0.2
DSR [34]	49.9±0.5	46.9±0.6	45.9±0.1	46.3±0.1	40.0±0.4	41.9±0.6	40.8±0.4	36.7±0.2	30.7±0.2	21.0±0.6	51.8±0.2	50.6±0.6	49.0±0.3	45.8±0.4	36.1±1.7	52.3±0.5	51.5±0.2	48.9±0.6	42.3±1.1	*
SNFS [45]	48.3±0.3	48.5±0.7	48.3±0.4	46.8±0.1	41.2±0.3	46.0±0.9	42.2±0.2	35.3±0.6	21.2±0.4	11.0±0.2	53.2±0.7	51.7±0.1	49.9±1.3	45.9±0.0	33.7±0.7	50.9±0.0	50.7±0.5	48.1±0.3	43.8±0.4	*
RigL [14]	46.4±0.4	46.8±0.2	45.7±0.2	43.7±0.3	37.8±0.3	46.6±0.7	43.7±0.2	38.1±0.2	31.6±0.2	19.8±1.6	52.6±0.3	52.6±0.0	50.8±0.1	47.2±0.4	38.9±0.7	51.2±0.4	51.1±0.4	49.6±0.2	46.7±0.2	32.5±1.2
SET-ITOP [32]	46.4±0.2	46.6±0.4	45.3±0.4	42.8±0.2	36.3±0.4	46.5±0.2	44.5±0.4	38.7±0.5	31.9±0.2	22.0±0.4	52.3±0.6	52.4±0.3	51.0±0.2	47.9±0.6	40.2±0.6	51.4±0.4	51.4±0.2	50.6±0.3	46.6±0.5	39.3±0.2
Dense (Baseline)			46.1±0.4					48.6±0.2										54.1±0.3		

C Graph Encoding Pooling Layers

Suppose the network has two consecutive layers l_i and l_{i+1} and a pooling operation ρ is employed between them. The two layers have respectively a bipartite graph representation G_i and G_{i+1} . However, the MGE is not directly applicable since $|R_i| \neq |L_{i+1}|$. Nevertheless, we know a priori that $|\rho(R_i)| = |L_{i+1}|$. This encoding extension aims at generating a second version of G_i , called G'_i , such that $|L'_i| = |L_i|$ and $|R'_i| = |\rho(R_i)|$. In a nutshell, the second layer of the bipartite graph corresponds to the output size after the pooling operation. The edge construction is straightforward: each node in the pooling window p_w , which is computed over R_i , is linked with a node $x \in R'_i$, and all the edges going from L_i to the nodes in p_w are connected to x . Then, based on such pooling encoding, any pair of consecutive layers G'_i and G_{i+1} can be linked together in the MGE since $|R'_i| = |L_{i+1}|$.

D Extended Results

In this section, we include all the extended results for our classification and regression analysis.

D.1 Classification

In the main paper, we showed in Table 5 the classification accuracy both for pruning algorithms and categories thereof. Here, we include the feature importance, for the *combination* setting which considers all the metrics together, for both cases, using permutation importance. In Figure 3, we plot the feature importance for pruning category classification, while in Figure 4 the results regarding pruning algorithm classification are shown.

Considering the algorithm category classification, it is worth mentioning how the clusters (i.e., the number of connected components) turn out to be the most discriminative feature for the Sparsity-wise case. The results are slightly different for the Architecture-wise case, where instead the most discriminative metrics change based on the architecture (as already discussed in Section 5).

As for the pruning algorithm classification, in the Sparsity-wise setting the most discriminative features turn out to be the fraction of disconnected nodes and the stability metrics, while for the Architecture-wise case, the feature importance still depends on the architecture selected as in the pruning category case.

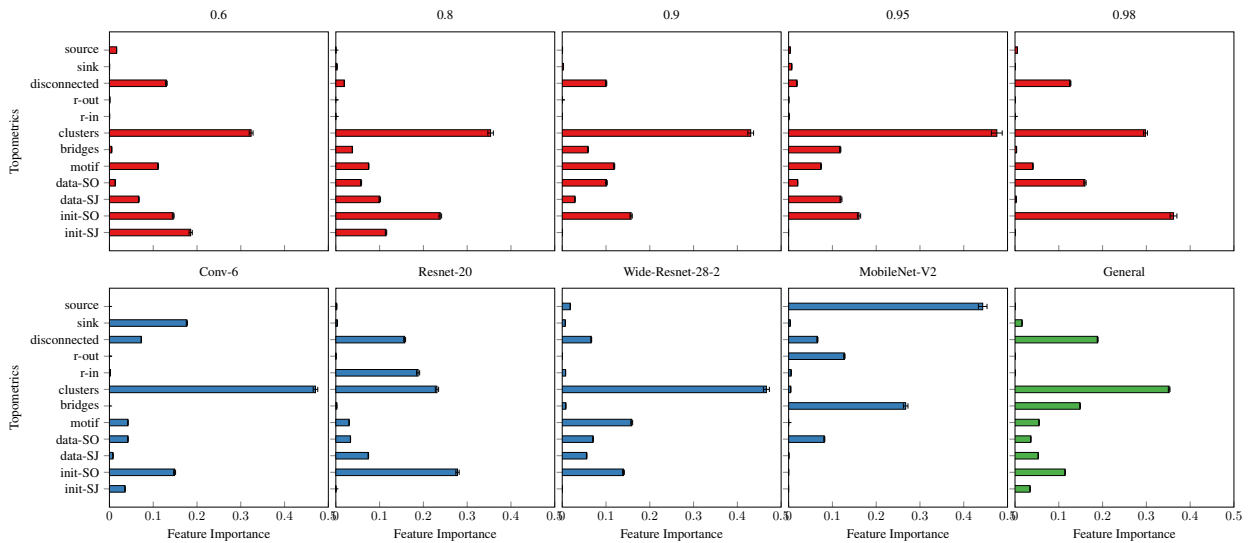


Figure 3: Feature importance for the pruning category classification for Sparsity-wise (red), Architecture-wise (blue), and General (green) cases.

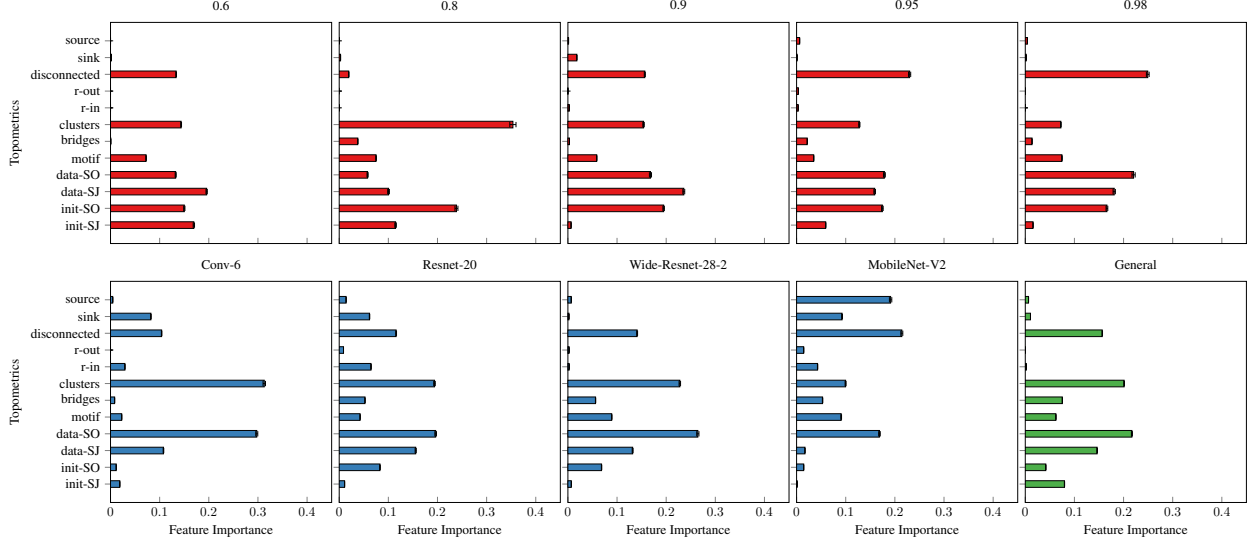


Figure 4: Features importance for the pruning algorithm classification for Sparsity-wise (red), Architecture-wise (blue), and General (green) cases.

D.2 Regression

In the main paper, in Table 6 we showed the R^2 coefficient using the *combination* of all the metrics. Here, we also provide in Table 12 the correlation coefficient obtained using each category of topometrics (*local*, *regional*, and *stability*) by itself.

Table 12: R^2 computed using stratified k-fold with $k = 5$ over 100 runs using *local*, *regional*, and *stability* as topometrics.

Dataset	Topometrics	R^2 (Sparsity-wise)					R^2 (Architecture-wise)			
		0.6	0.8	0.9	0.95	0.98	Conv-6	Resnet-20	Wide-Resnet-28-2	MobileNet-V2
CIFAR-10	Local	.50±.05	.36±.08	.23±.12	.42±.14	.49±.10	.55±.09	.72±.06	.40±.09	.77±.07
	Regional	.72±.03	.74±.05	.79±.04	.83±.06	.70±.08	.96±.01	.84±.07	.94±.02	.90±.06
	Stability	.43±.07	.28±.08	.31±.08	.05±.08	.22±.11	.84±.03	.62±.04	.71±.05	.73±.06
CIFAR-100	Local	.02±.03	.06±.07	.35±.13	.44±.11	.55±.09	.50±.10	.83±.02	.60±.07	.77±.09
	Regional	.35±.07	.59±.07	.74±.06	.65±.08	.60±.10	.95±.01	.91±.02	.91±.03	.94±.02
	Stability	.21±.10	.40±.12	.38±.12	.29±.13	.35±.11	.73±.07	.74±.03	.70±.08	.69±.09
Tiny-ImageNet	Local	.04±.05	.13±.09	.28±.09	.45±.08	.84±.03	.64±.06	.76±.02	.60±.06	.76±.13
	Regional	.53±.10	.85±.07	.82±.06	.66±.08	.63±.12	.92±.03	.92±.02	.90±.03	.92±.04
	Stability	.29±.13	.32±.13	.31±.10	.46±.08	.31±.08	.76±.08	.61±.05	.84±.05	.55±.14

Furthermore, while in the main paper (in Figure 2) the feature importance of each metric was averaged over all the three tested datasets, here we show the feature importance separately for each dataset. The results are available in Figure 5 for the Sparsity-wise case and in Figure 6 for the Architecture-wise case.

E Extended Topometrics Analysis

In this section, we report the trend of each topometric for each category (i.e., *local*, *regional*, and *stability*) when changing the sparsity ratio for each model. The results have been average over the three tested datasets. We show the trends both when the pruning algorithms are grouped by category, see Figures 7-9, and separately for each algorithm, see Figures 10-12.

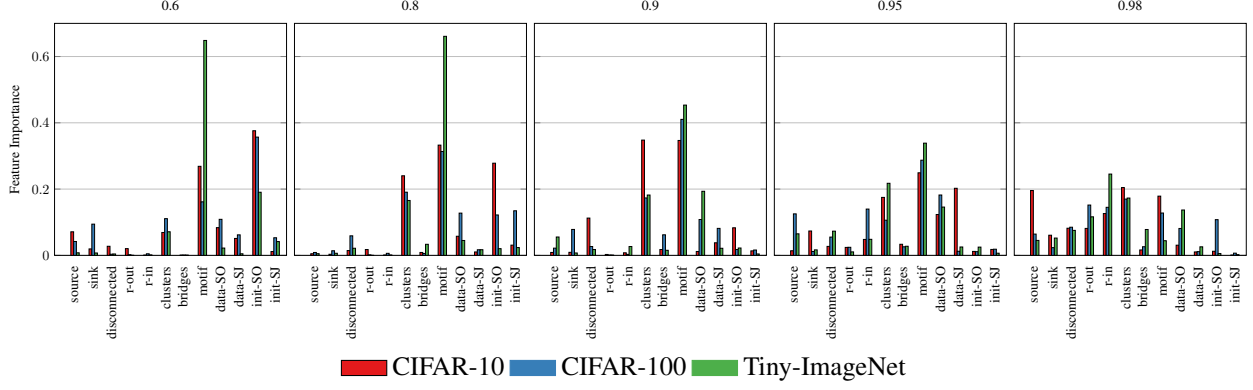


Figure 5: Feature importance using the *combination* of all metrics for the Sparsity-wise case. See Table 6 for the numerical details.

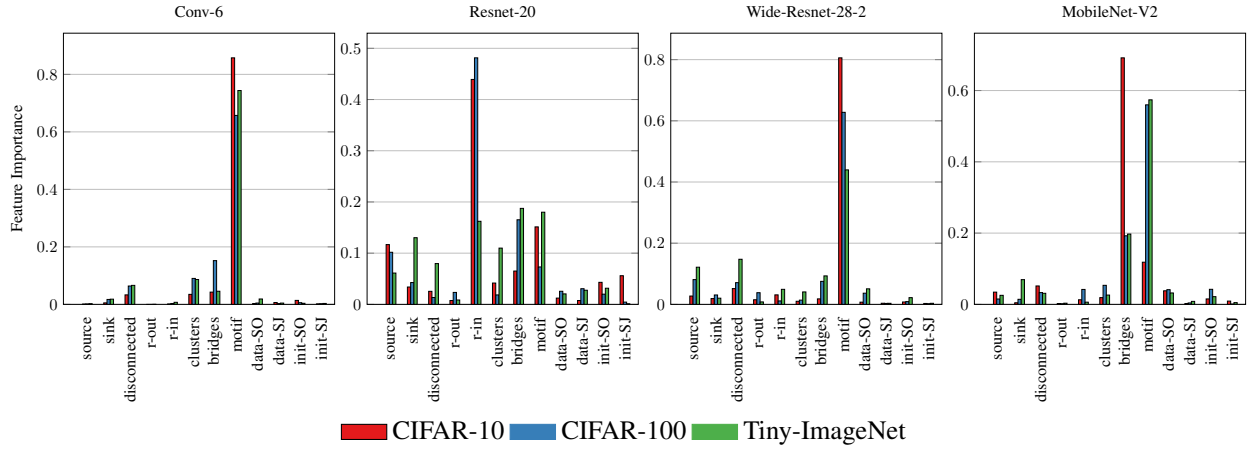


Figure 6: Feature importance using the *combination* of all metrics for the Architecture-wise case. See Table 6 for the numerical details.

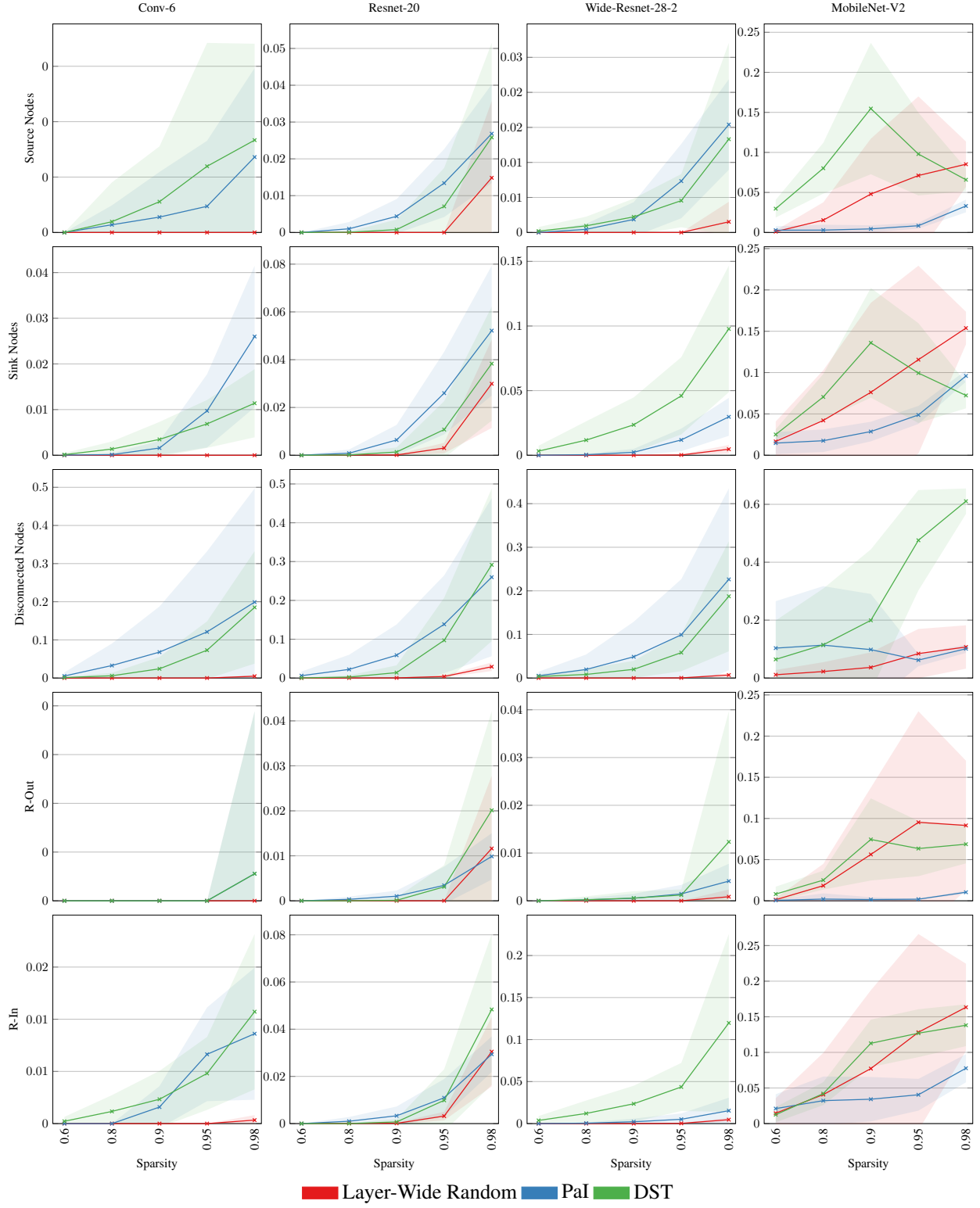


Figure 7: *Local* metrics trends for each pruning category.

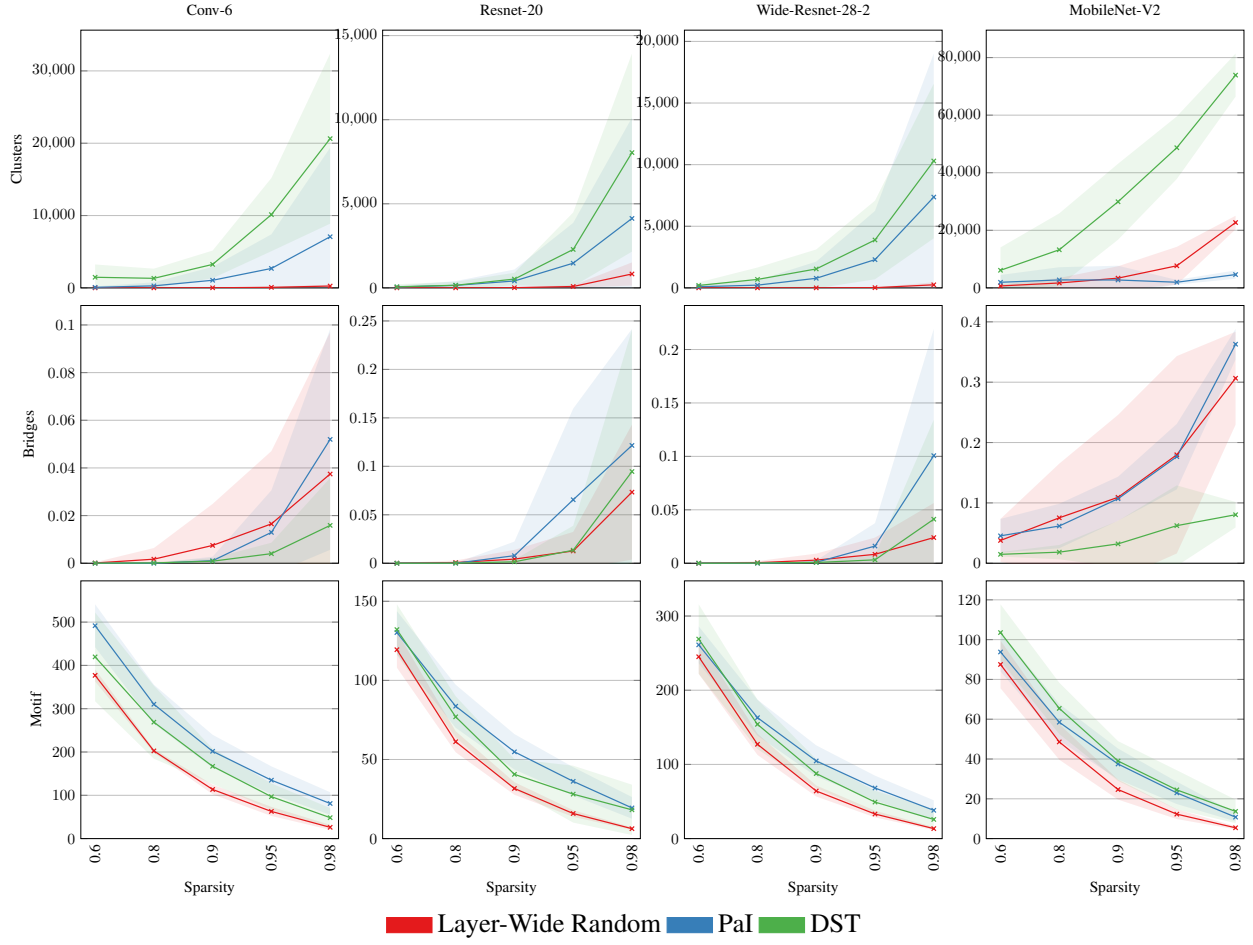


Figure 8: *Regional* metrics trends for each pruning category.

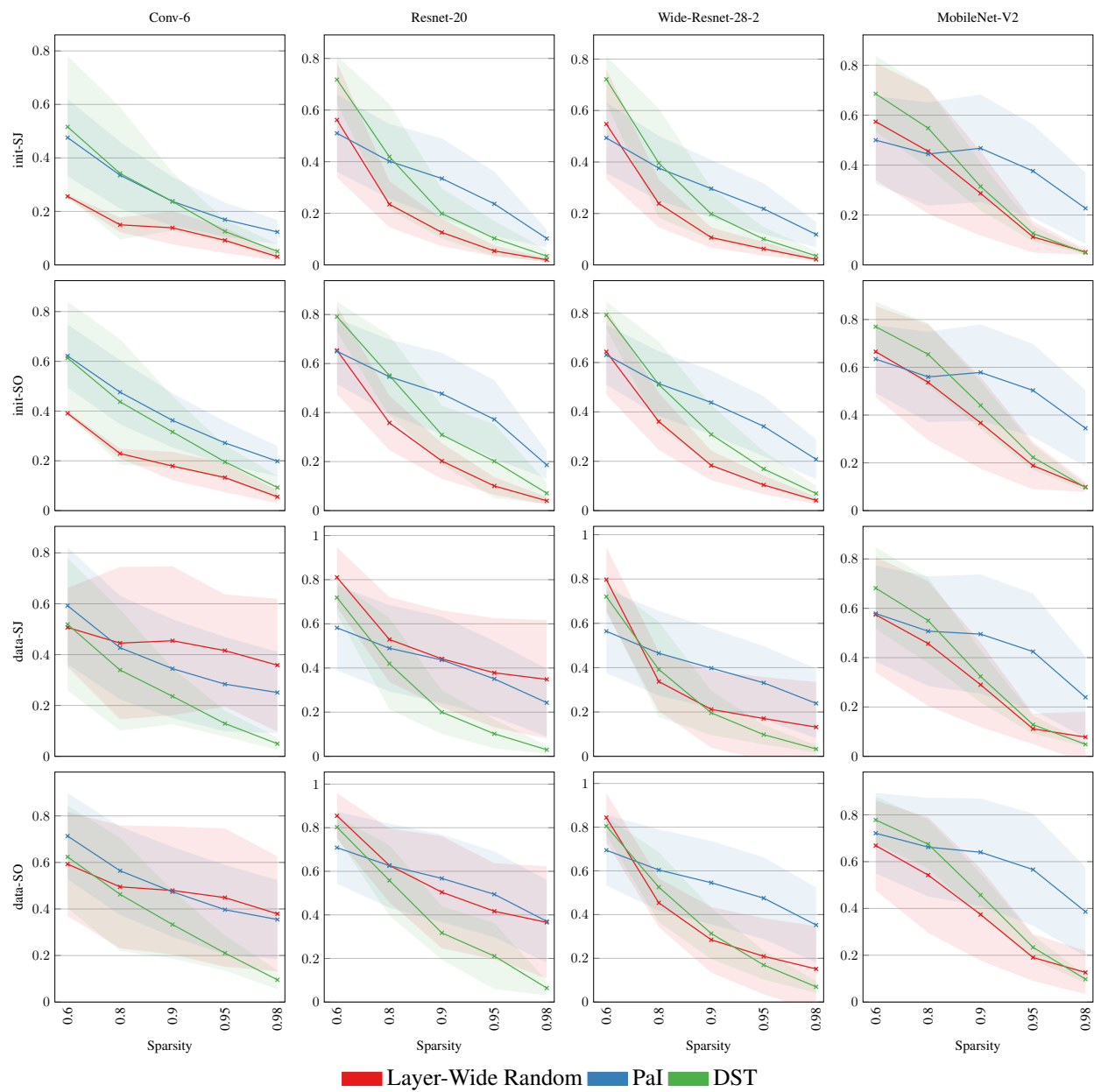


Figure 9: *Stability metrics trends for each pruning category.*

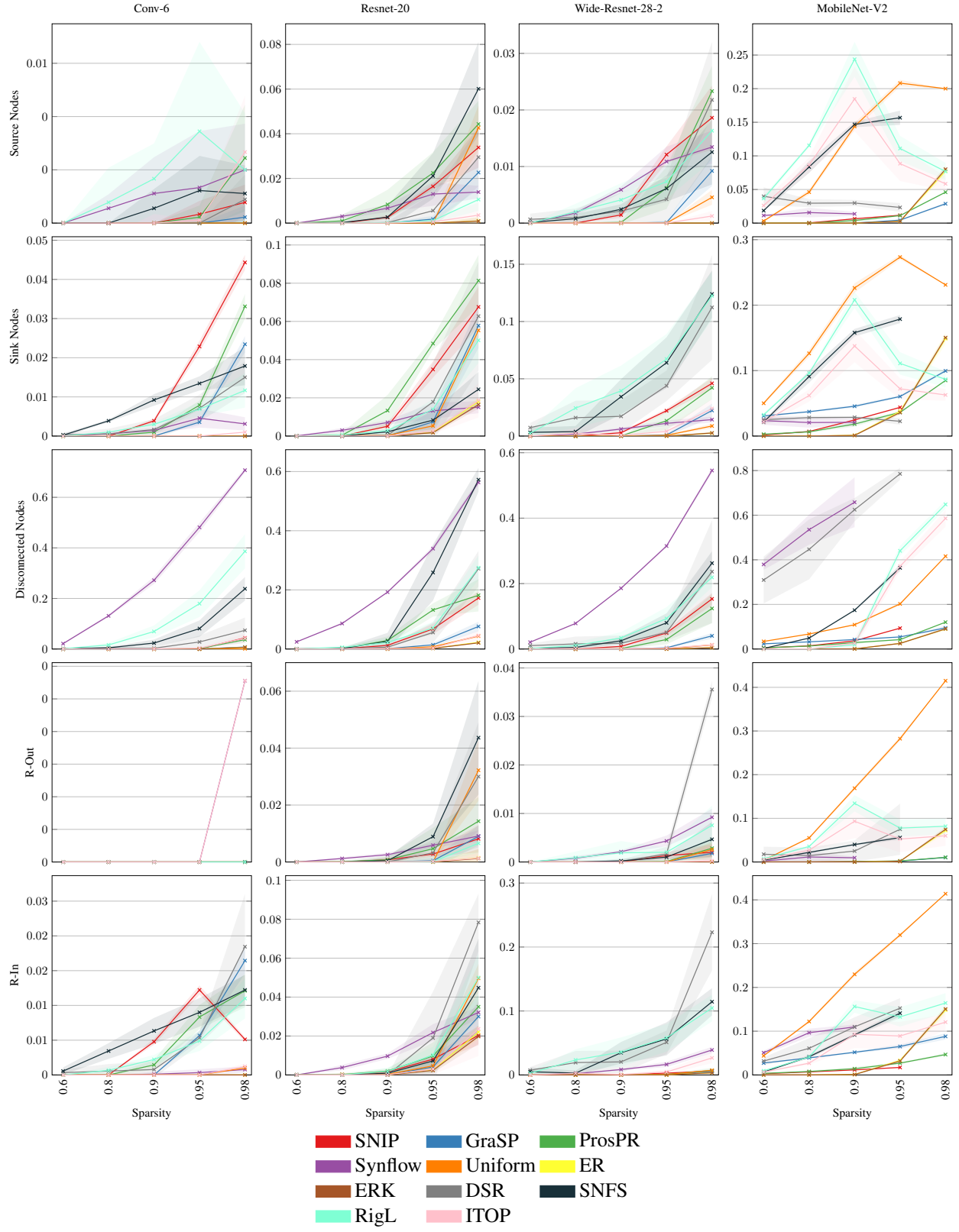


Figure 10: *Local* metrics trends for each pruning algorithm.

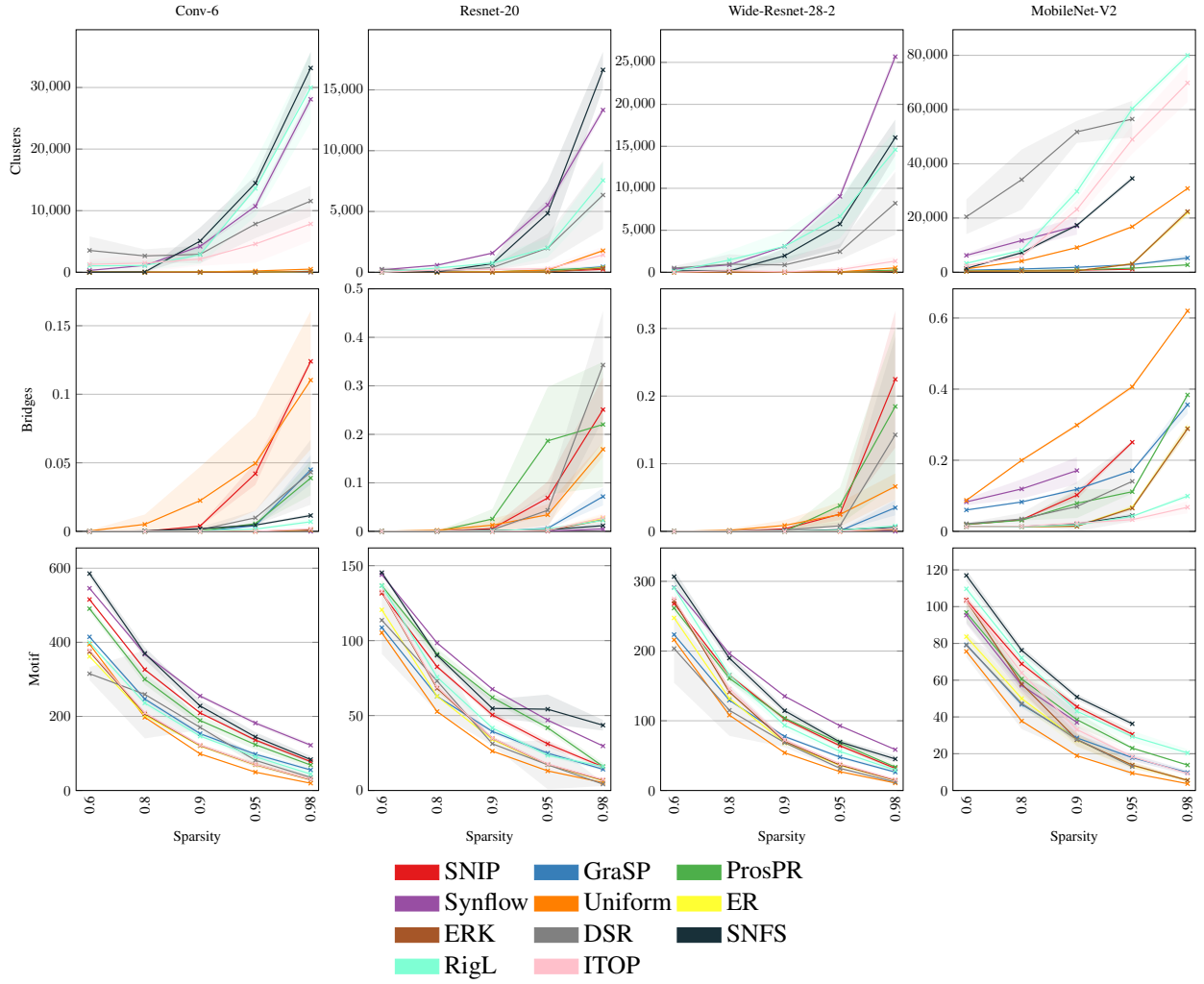


Figure 11: *Regional* metrics trends for each pruning algorithm.

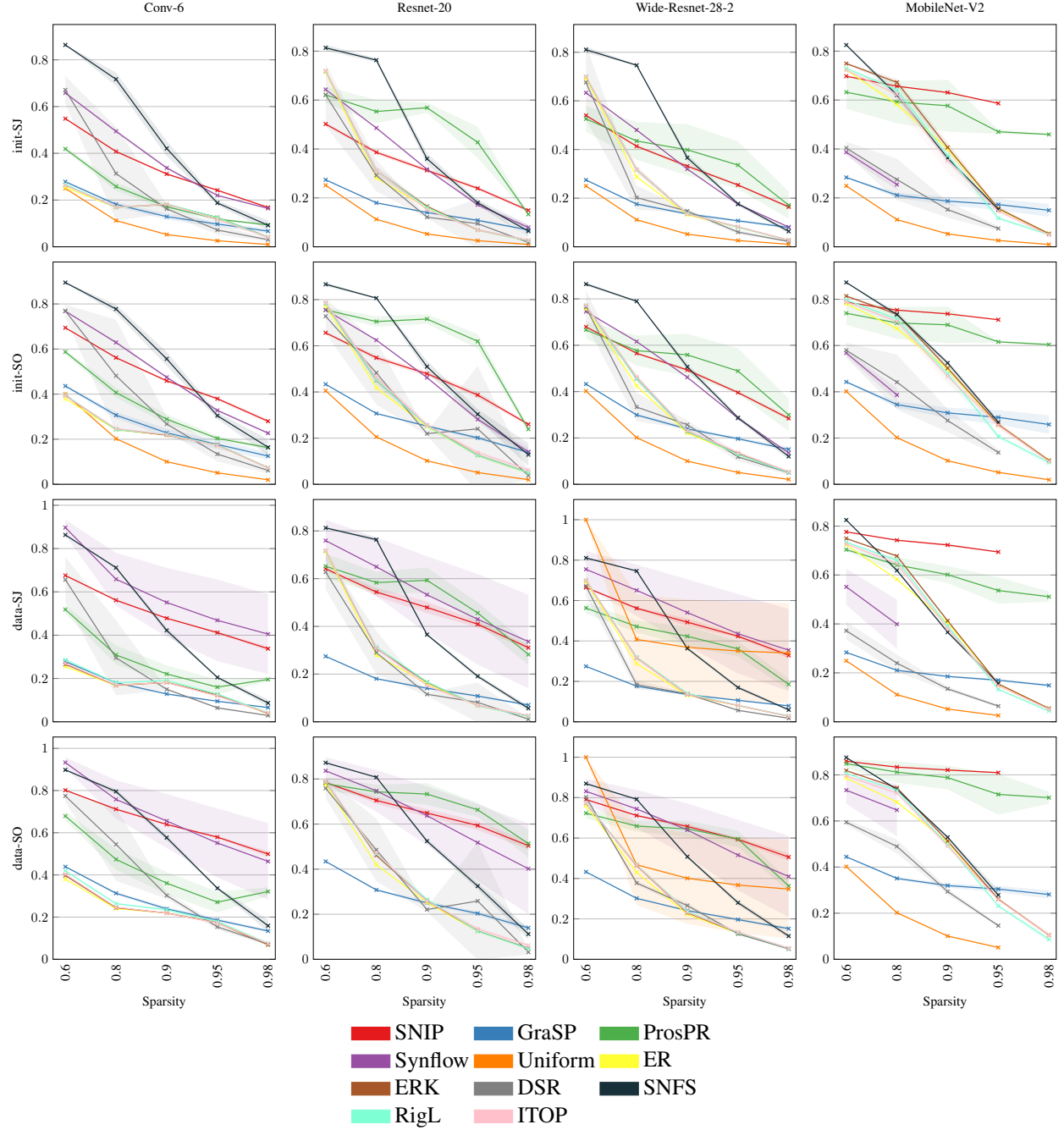


Figure 12: *Stability metrics trends for each pruning algorithm.*

F Graph Encoding Visualization

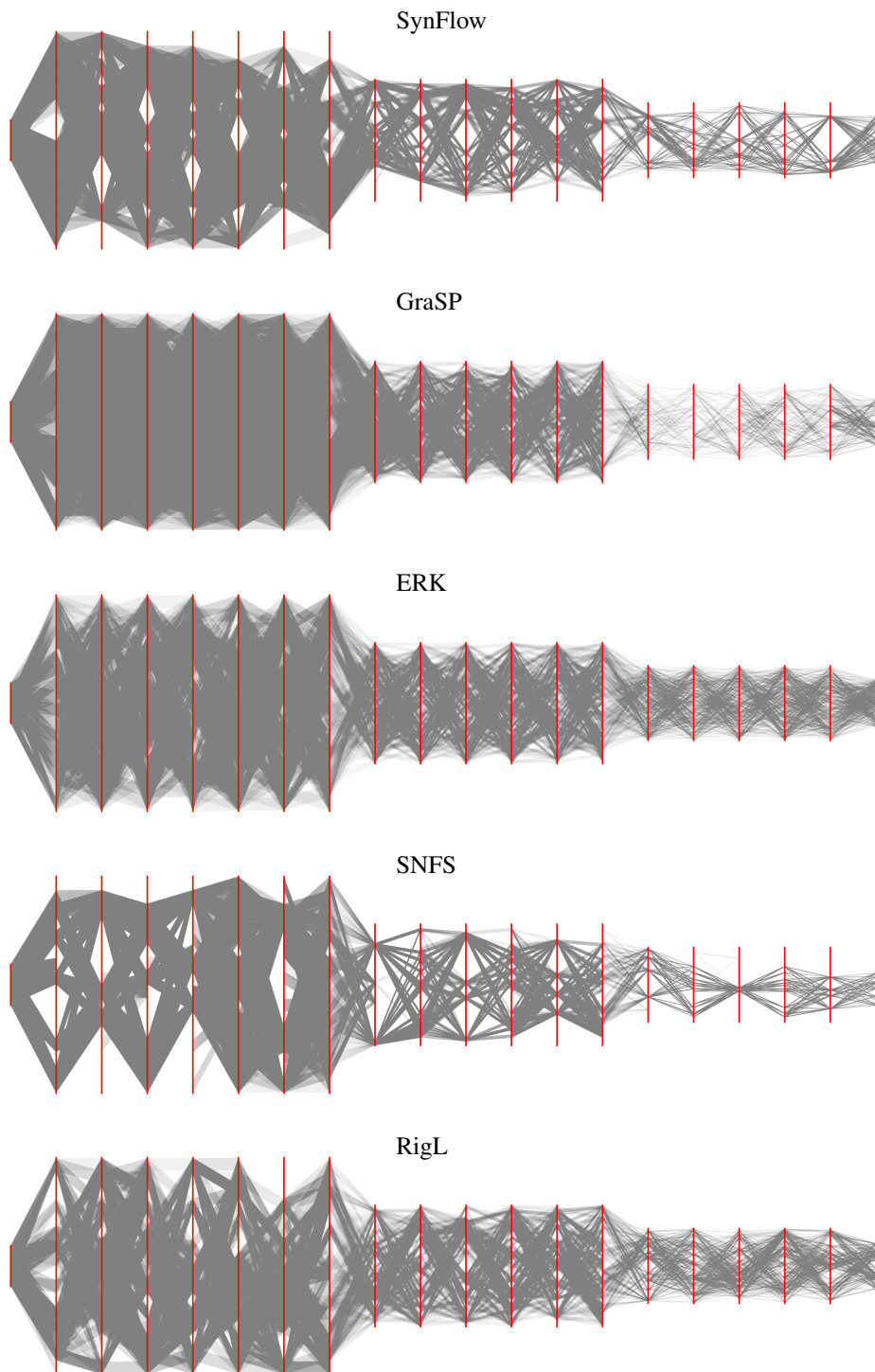


Figure 13: Visual representation of the proposed Multipartite Graph Encoding (MGE) for sparse Resnet-20 architectures with input size 32×32 , obtained using five different pruning algorithms with a sparsity ratio of 0.98. The networks have been initialized with the same seed. The last classification (linear) layer, as well as the residual connections, are omitted for conciseness.